Energy & Environmental Science

RSC Publishing

REVIEW

View Article Online
View Journal | View Issue

Cite this: *Energy Environ. Sci.*, 2013, **6**, 2390

Highly efficient organic tandem solar cells: a follow up review

Tayebeh Ameri,*[a] Ning Li[a] and Christoph J. Brabec[ab]

Multi-junction solar cell configurations, where two or further sub-cells with complementary absorption are stacked and connected in series or parallel, offer an exciting approach to tackle the single junction limitations of organic solar cells and further improve their power conversion efficiency. In this article we aim to follow up our previous work and review the most important and novel developments that have been recently reported on organic tandem solar cells. In addition, some brief theoretical considerations addressing the potential of single and tandem solar cells, the working principles of the intermediate layer, the importance and benefits of optical simulations and finally the intricacies of a precise performance measurement of bulk-heterojunction organic tandem solar cells based on complementary absorber materials are presented.

Received 3rd February 2013
Accepted 21st May 2013

DOI: 10.1039/c3ee40388b

www.rsc.org/ees

Broader context

Organic photovoltaics (OPVs) by attracting enormous research interest in the last decade have occupied an important position in the future renewable energy strategy. The power conversion efficiency (PCE) of OPV devices has exceeded the 10% milestone. The high efficiency along with the advantages of low cost, flexibility, ease of manufacture, *etc.* can represent the broad prospects of commercial applications for OPVs. Tandem concept is one of the most promising approaches to tackle the main losses in single junction OPV devices, such as narrow absorption window and thermalization losses. The PCE of tandem OPV devices is predicted to approach or even exceed 15% by connecting two sub-cells with different absorption spectra. Owing to the rapid development of novel materials and techniques, the PCE of organic tandem devices has been increased up to 12% since our previous work in 2009. In this contribution, the recently reported highly efficient tandem devices are reviewed and important aspects like the design of efficient intermediate layers, precise light-management, meticulous device optimization and reliable characterization methods, required to further promote the performance of tandem OPV devices, are discussed in detail.

1 Introduction

Addressing climate change, pollution and energy insecurity problems all at once requires major changes in our energy infrastructure. Over the past decade, a number of studies have proposed large-scale renewable energy plans, mainly based on wind, water and sunlight resources.[1–4] As shown in Fig. 1,[5] the solar energy resource dwarfs potentially all other renewable and fossil-based energy resources combined. The yearly sustainable renewable supply of solar energy received by the emerged continents alone is more than 30 times larger than the total planetary reserves of coal and 1500 times larger than the current planetary energy consumption.[1] Therefore, photovoltaic (PV) technology is the object of steadily growing interest from both academic and industrial protagonists.

After the world-wide photovoltaic market more than doubled in 2010, the market grew again by almost 30% in 2011, despite difficult economic conditions. In 2011, the photovoltaic industry production reached a world-wide production volume of around 35 GW and another moderate increase is expected for 2012. Yearly growth rates over the last decade were on average more than 40%, which makes the photovoltaic industry one of the fastest growing industries at present.[6,7] The most rapid growth in annual production over the last five years could be observed in Asia, where China and Taiwan together now account for almost 65% of world-wide production (Fig. 2a). With a cumulative installed capacity of over 66 GW, the European Union is leading in PV installations with 2/3 of the total world-wide almost 100 GW of solar photovoltaic electricity generation capacity at the end of 2012 (Fig. 2b). The wafer-based silicon solar cells are still the main technology and have around 85% market shares.[6] The challenge facing the photovoltaic industry is cost effectiveness through much lower embodied energy. Although the cost of photovoltaic systems, especially in the last two years, has significantly reduced, solar power in comparison with fossil energy sources is still expensive. To bridge this difference in costs and make solar power a primary energy source of our society, the solar industry is working on the consistent further development of existing technologies and on the exploration of new solar technologies.

[a]*Institute of Materials for Electronics and Energy Technology (I-MEET), Department of Materials Science and Engineering, Friedrich-Alexander University Erlangen-Nuremberg, Martensstrasse 7, 91058 Erlangen, Germany. E-mail: tayebeh.ameri@ww.uni-erlangen.de*

[b]*Bavarian Center for Applied Energy Research (ZAE Bayern), Am Weichselgarten 7, 91058 Erlangen, Germany*

Among all the alternative technologies, the thin-film approach deserves to gain more attention and is likely to represent about 26% of the overall production by 2015.[6] All the attractive and beneficial features of organic materials such as their strong absorption coefficient, ease of processing, mechanical flexibility and ability to tailor the bandgap, have brought them into the focus of attention for thin-film PV applications. Organic solar cells (OSCs) represent a new technology that could lead to the most significant cost reduction in the mid-long term.[8–11] Various printing and coating techniques such as inkjet, slot die, screen, gravure, spray and others are established and already demonstrated for OPV production. The attractive feature of these printing and coating methods is their high production speed of up to several meters per second. With a single production line some 100 000 m^2 of film per day can be produced, which at an efficiency of 5% (*i.e.* 50 W m^{-2}) corresponds to a daily capacity of 5 MW. Therefore, a single printing or coating facility could produce modules with the production energy volume of over 1 GW per year.[12,13] Obviously, the printing and coating processes are orders of magnitude more productive than the currently largest production facilities for silicon-based PVs. In addition, the investment on the printing equipment is many times cheaper than for conventional inorganic solar technologies. This illustrates the potential of printed solar power which can be also easily set up at different locations.

Recently, a large number of organic solar cells with power conversion efficiencies (PCEs) beyond 6% and up to 10% were reported, making this topic more than ever promising.[14–16] However, there is still significant room with respect to research and development necessary to make high-performance organic solar cells ready for the market. In this regard, various strategies are currently in the exploration phase at different levels of maturity. Among them, the well-known concept of tandem solar cells is one of the most promising approaches to tackle the main losses in single junction OPV devices and improve the device performance.

Tayebeh Ameri received her MSc in Solid State Physics from Ferdowsi University of Mashhad, Iran. In May 2006, she joined Konarka Austria to study for a PhD under the supervision of Prof. Christoph. J. Brabec (Konarka) and Prof. Kurt Hingerl (Johannes Kepler University Linz, Austria). She received her PhD in Engineering Sciences in 2010. Since October 2010, she has been a postdoctoral fellow in the group of Prof. Brabec in the institute of Materials for Electronics and Energy Technology (i-MEET) at the Friedrich Alexander University Erlangen-Nürnberg, where she is also leading the organic photovoltaics team. Her main research interests include investigation and development of ternary and tandem organic solar cells.

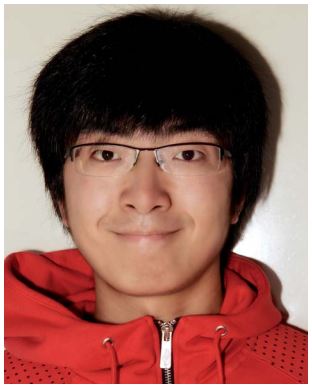

Ning Li is currently a PhD student under the supervision of Prof. Christoph J. Brabec at the institute of Materials for Electronics and Energy Technology (i-MEET) at Friedrich Alexander University Erlangen-Nuremberg (FAU). He received his BSc and MSc degrees in Materials Science and Engineering from Tongji University (2008) and FAU (2010), respectively. His research is focused on the organic tandem solar cells.

Christoph J. Brabec is holding the chair "Materials for Electronics and Energy Technology (i-MEET)" at the materials science department of the Friedrich Alexander University Erlangen-Nürnberg. Further, he is the scientific director of the Erlangen division of the Bavarian research institute for renewable energy (ZAE Bayern, Erlangen), board member of the ZAE Bavaria and board member of the Energy Campus Nurnberg. He received his PhD (1995) in physical chemistry from Linz university, joined the group of Prof. Alan Heeger at UCSB for a sabbatical, and continued to work on all aspects of organic semiconductor spectroscopy as assistant professor at Linz university with Prof. Serdar Sariciftci. He joined the SIEMENS research labs as project leader for organic semiconductor devices in 2001, finished his habilitation in physical chemistry in 2003 at Linz university and joined Konarka in 2004, where he was holding the position of the CTO before joining the university. He is the author and co-author of more than 200 papers and nearly 100 patents and patent applications. His research interests are organic photovoltaics, all aspects of solution processed semiconductors and technologies for renewable energy scenarios.

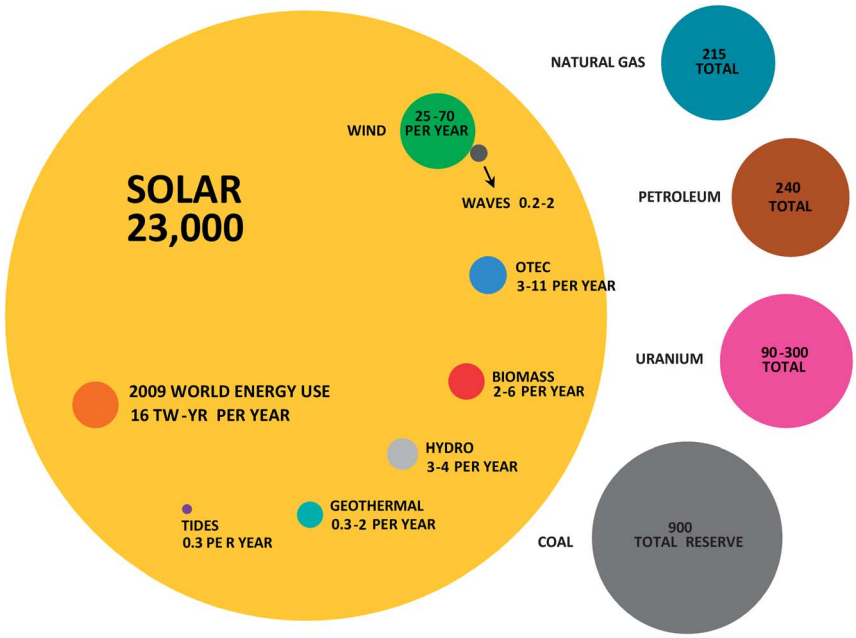

Fig. 1 Comparison of finite and renewable planetary energy reserves (Terawatt-years). Total recoverable reserves are shown for the finite resources. Yearly potential is shown for the renewables.[5]

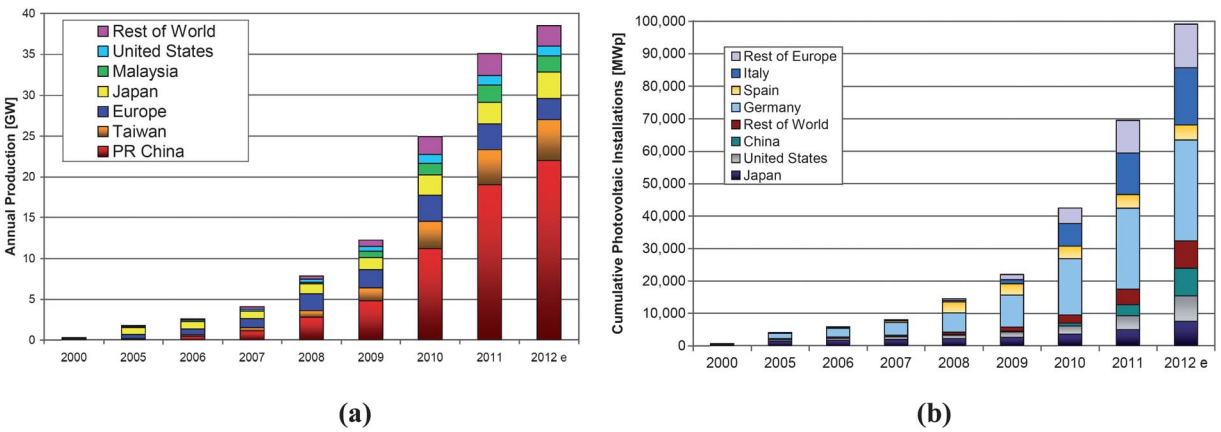

Fig. 2 (a) World photovoltaic cell/module production from 2000 to 2012 and (b) cumulative photovoltaic installations from 2000 to 2012.[6]

In this article, we aim to follow up our previous work[17] and review the most important and novel developments that have been recently reported on organic tandem solar cells. In the first part, we introduce some brief theoretical considerations addressing the potential of single and tandem solar cells. The working principles and importance of the intermediate layer are explained as an important subject for full functional tandem solar cells. Furthermore, the benefits of optical simulations to verify the ultimate efficiency potential of novel materials are discussed. Then, we present and discuss the experimental achievements with considerably high performance reported in the literature from 2007 to present. Finally, we discuss the intricacies of the precise performance measurement of bulk-heterojunction (BHJ) organic tandem solar cells based on complementary absorber materials and describe the applicable method in this regard.

2 Fundamental limitations

Understanding the fundamental limitations of photovoltaics will lead to the achievement of a systematic approach toward further developments of the solar cell technologies. Although the theoretical considerations of photovoltaics have already been described in detail in our previous review, their importance encourages us to address them briefly here as well.

2.1 Single junction solar cells

The fundamental limitations of the energy conversion efficiency of a solar cell are mainly based on the thermodynamical losses. In photovoltaics, only the photons having energy larger than the bandgap of a photoactive material can be absorbed and contribute to the energy conversion. On the other hand,

thermalization of the hot charge carriers is another important contributor to losses. Considering a light source of AM1.5G, the maximum efficiency (η) achievable with a material having a bandgap energy E_g is calculated by:

$$\eta(E_g) = J_{sc}(E_g) \times V_{oc}(E_g) \times FF \quad (1)$$

where FF is the fill factor (ideally equal to 1), V_{oc} is the open circuit voltage and J_{sc} is the short circuit current density which is calculated by:

$$J_{sc}(E_g) = e \int_{E_g}^{\infty} I_{ph}(E) \times EQE(E) \times dE \quad (2)$$

where $I_{ph}(E)$ given in s^{-1} m^{-2} J^{-1} contains the spectrum of the light source and EQE is the external quantum efficiency (ideally 1 for a photon absorbed). According to the basic investigation of Shockley and Queisser and considering the spectral losses alone, a solar cell has a peak theoretical efficiency of 48% for a material with E_g close to 1.1 eV.[18] Materials with a bandgap smaller than this suffer from reduction in the open circuit voltage (V_{oc}) and those with a bandgap larger than 1.1 eV are limited by the decrease of the short circuit current (J_{sc}). Including the effects of blackbody radiation and radiative/non-radiative recombination of charge carriers, the theoretical maximum efficiency reduces down to 30.1% for a single device under 1 sun illumination.[18] However, this basic calculation describes the fundamental limitations of a solar cell based on inorganic semiconductors. Organic solar cells face further restrictions due to the natural specifications of organic semiconductors.

In organic materials with a small dielectric constant, absorption is governed by Frenkel excitons. The binding energy of Frenkel excitons is around 0.3 eV and the exciton lifetime is typically of the order of ns.[19,20] Therefore to achieve substantial energy conversion efficiencies, these excited electron–hole pairs need to be dissociated into free charges with a high yield. Excitons can be dissociated at interfaces of materials with different electron affinities. Blending conjugated polymers (donor) with high electron affinity molecules (acceptor) like fullerene derivatives (PC60BM and PC70BM) has proven to be an efficient way for rapid exciton dissociation. It is shown experimentally that a minimum offset of 0.3 eV either between donor and acceptor's lowest unoccupied molecular orbital (LUMO) or highest occupied molecular orbital (HOMO) levels is required to achieve an efficient charge transfer between the two components.[21] Correspondingly, the V_{oc} is limited by the difference between the acceptor LUMO and the donor HOMO levels, which also defines the built-in field (V_{bi}). Considering a contact loss of another 0.3 eV,[22–24] the V_{oc} obeys the following empirical equation:[25]

$$V_{oc} = \frac{1}{e}\left(\left|E_{HOMO}^{donor}\right| - \left|E_{LUMO}^{acceptor}\right|\right) - 0.3 \quad (3)$$

For single junction organic solar cells with a donor having a bandgap energy of 1.5 eV, a practical efficiency of nearly 11% can be expected based on the following assumptions: a 0.6 eV loss in V_{oc} (accounting for the minimum required LUMO level offset and contact losses), taking into account absorption/internal quantum efficiency (IQE) limitations (assuming EQE = 65%) and charge carrier transport losses (assuming FF = 65%). In early April 2011, a new efficiency record of >10% from a solution processed small molecule was reported by Mitsubishi Chemical and certified by Newport.[26] This breakthrough did narrow significantly the performance gap between OPV technology and competitive thin film PV technologies, as shown in Fig. 3.

Fig. 4a summarizes the efficiency of donor/acceptor organic solar cells *versus* the bandgap energy of the donor and the LUMO offset between the two materials, assuming an EQE and FF of 65%.[25] This model can be used as a guideline for the material selection and material development for bulk-heterojunction solar cells. Obviously, the LUMO offset of the materials has an even more pronounced influence on device efficiency than the bandgap of the absorber. To go significantly beyond 10% efficiency, both EQE and FF need to be improved. This would shift the efficiencies shown in Fig. 5a to higher values, but does not change the shape of the contour plot.

2.2 Tandem solar cells

The performance limitation of single junction devices is released by employing tandem devices. Tandem or multi-junction devices tackle simultaneously absorption and thermalization losses by absorbing the higher energy photons in a wide bandgap cell (higher voltage and lower photocurrent) and the lower energy photons in a smaller bandgap cell (lower voltage and higher photocurrent). The detailed balance limit of the performance of a tandem structure was investigated by De Vos in 1980.[27] The optimal combination of bandgaps for multi-junction structures reaches 42 to 53% efficiencies by increasing the number of stacked cells from 2 to 4 sub-cells. Currently, a device based on InGaP/GaAs/InGaAs with an

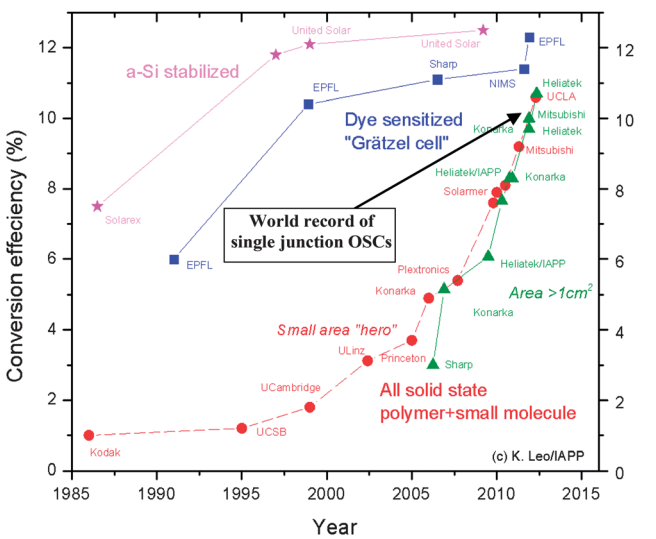

Fig. 3 Comparison of the world records between thin-film PV technologies of a-Si (stars), dye sensitized (squares) and organic solar cells (circles and triangles) from 1985 to present [source of picture: http://www.orgworld.de].

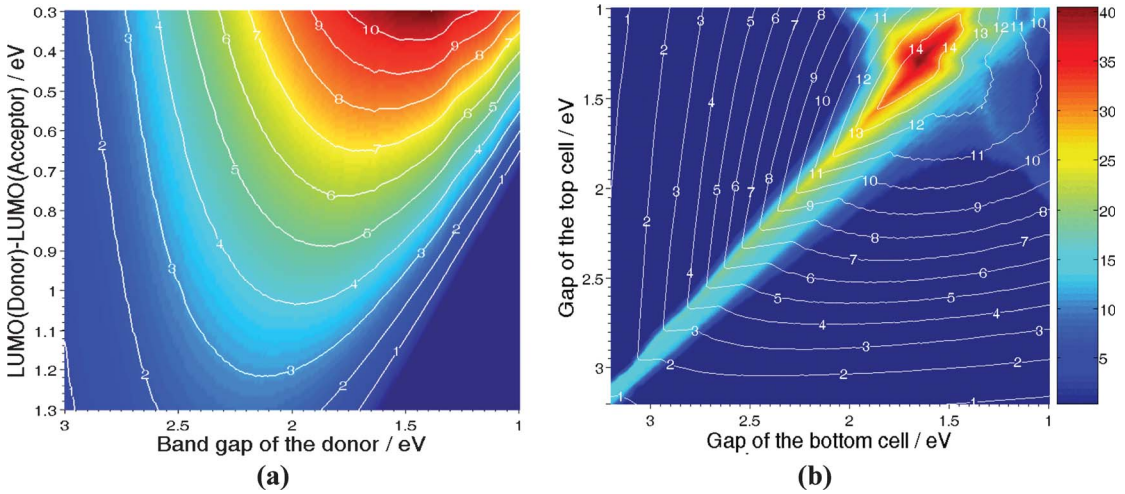

Fig. 4 (a) Efficiency of a donor–acceptor organic solar cell *versus* the bandgap energy of the donor, and the LUMO offset between the two materials.[25] Reprinted with permission from ref. 25, Copyright 2006, Wiley-VCH. (b) Efficiency of a donor–acceptor tandem organic solar cell made of two sub-cells stacked in series *versus* the bandgap energy of the top and bottom donors; both top and bottom donor–acceptor couples are assumed to have a LUMO offset of 0.3 eV.[28] Reprinted with permission from ref. 28, Copyright 2008, Wiley-VCH.

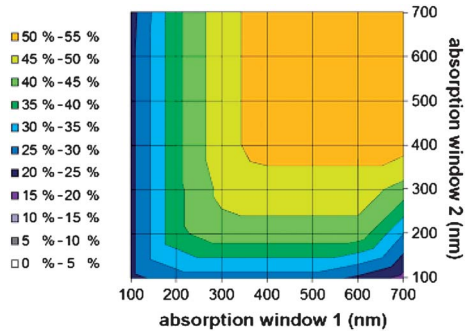

Fig. 5 The maximum efficiency in the ideal scenario for an organic tandem cell as a function of the absorption windows of the sub-cells. "Absorption window 1" refers to the bottom sub-cell with the highest absorber bandgap, directed at the sun.[34]

efficiency of 37.7 ± 1.2% and an active area of 1.047 cm^2 possesses the certified world record of multi-junction solar cells under AM1.5G.[26]

In an approach similar to the one applied for single junction cells, Dennler *et al.*[28] investigated the maximum efficiency possible for organic tandem cells. In this study, both top and bottom donor–acceptor couples were assumed to have a LUMO offset of 0.3 eV and the LUMOs of the first donor (E_{LUMO1}) and the second donor (E_{LUMO2}) were fixed to −4 eV, which is the optimum value for bulk heterojunction composites with PC60BM as the acceptor. An ideal fully transparent intermediate layer placed between the sub-cells was assumed to ensure a loss-free recombination of charge carriers in the intermediate layer. The V_{oc} of the tandem cell is then calculated as the sum of the respective V_{oc} of both sub-cells.

$$V_{oc,tandem} = V_{oc,bottom} + V_{oc,top} \quad (4)$$

An EQE of 65% and an IQE of 85% were considered constant over the absorption region of both sub-cells. As a result, the J_{sc} of bottom and top sub-cells is calculated as:

$$J_{sc,bottom}(E_{g,1}) = e\int_{E_{g,1}}^{\infty} I_{ph}(E) \times EQE_1(E) \times (1 - mirror_{loss}) \times dE \quad (5)$$

$$J_{sc,top}(E_{g,2}) = e\int_{E_{g,2}}^{\infty} I_{ph}(E) \times EQE_2(E) \times \left[1 - \frac{EQE_1(E)}{IQE_1(E)} \times (1 - mirror_{loss})\right] \times dE \quad (6)$$

where $E_{g,1}$ is the bandgap energy of the donor used in the bottom sub-cell, $E_{g,2}$ the bandgap energy of the donor used in the top sub-cell, I_{ph} the flux of photons in AM1.5G and EQE_1/IQE_1 absorption of the bottom sub-cell. $Mirror_{loss}$ represents the loss of absorption in the cell implemented in the tandem *versus* the stand-alone single cell that would have a perfect mirror as a top electrode. This loss is induced by the absence of significant reflection at the interface between the bottom sub-cell and the intermediate layer. Depending on the thickness of the bottom sub-cell, these losses were estimated to be about 15% on average, according to detailed optical simulations based on the transfer matrix formalism (TMF).[28] Tandem operation requires the current densities of both sub-cells to be matched at the maximum power point. Assuming further that the FFs of the single sub-cells are identical, as well as their shunt resistances, Kirchoff's law predicts that the short-circuit current density of a tandem cell is equal to the smaller J_{sc} of the single cells.

$$J_{sc,tandem} = \min[J_{sc,bottom}, J_{sc,top}] \quad (7)$$

Based on this consideration, the maximum efficiency of an organic tandem solar cell can be calculated as a function of the bandgaps, as presented in Fig. 4b. This calculation suggests that tandem cells have a 30% higher efficiency potential as compared to single junction devices. Fig. 4b shows that a

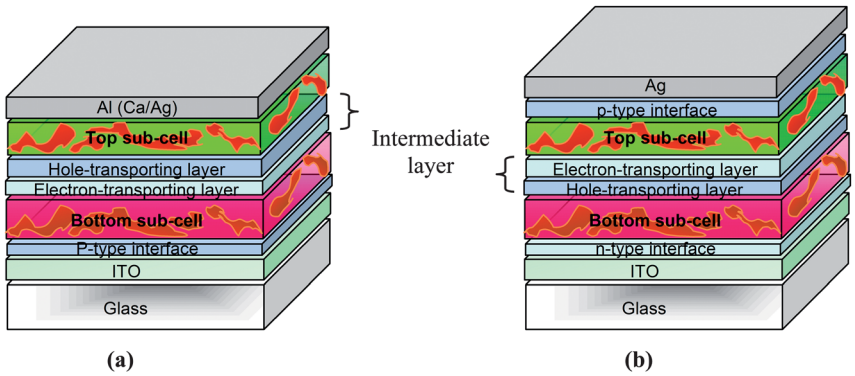

Fig. 6 Schematic representation of an organic tandem device comprised of two sub-cells having different, complementary absorption spectra in a normal (a) and an inverted configuration (b).

maximum efficiency of up to 15% can be achieved by combining a bottom donor having a bandgap of 1.6 eV with a top donor having a bandgap of 1.3 eV. Under the given assumptions, the most efficient tandem cells require materials with a bandgap energy difference of only 0.3 eV.

In this work as well as some other studies,[29–33] the narrow absorption window, characteristic of organic materials, is not considered. When calculating the potential of organic (single and multi-junction) solar cells, Minnaert and Veelaert[34] investigated the influence of different spectral absorption widths on the efficiency potential of organic tandem and triple-junction solar cells. According to their simplified model, the efficiency decreases rapidly as soon as one sub-cell has a low absorption window. The maximum efficiency of an organic tandem cell as a function of the absorber's spectral width of the sub-cells is presented in Fig. 5. Interestingly, this study suggests that it would not pay off to try developing organic materials with an absorption window broader than 400 nm. More than 90% of the absolute maximum efficiency can be achieved by having absorbers with a spectral width of 400 nm for both sub-cells. In addition, the optimum bandgap of the cells shifts towards higher energies for narrower absorption windows. Similar conclusions were drawn for the efficiency potential of triple-junction solar cells as a function of the different absorption windows of the three sub-cells.

Fig. 6 shows the most frequently reported configurations of organic tandem solar cells. Indeed, the two cells involved in the device can be connected either in series (two-terminal) or in parallel (three-terminal) depending on the nature of the intermediate layer and on the way the intermediate layer and the two electrodes are connected. In the vast majority of reports though, the series-connection is used. In this case, the device can be fabricated in the conventional (or normal) architecture or in the inverted one,[35] as depicted in Fig. 6a and b respectively. The intermediate layer has to ensure the alignment of the quasi-Fermi level of the acceptor of the bottom cell with the quasi-Fermi level of the donor of the top cell (or *vice versa* for an inverted architecture). Following the same principle, an infinite number of devices can be theoretically piled up this way.

3 Working principles of the intermediate layers

In the context of photovoltaic operation, free charge carriers generated in the active layer are selectively extracted through an electron-transporting layer (ETL) at the cathode or a hole-transporting layer (HTL) at the anode. Depending on the tandem architecture, a semi-transparent electrode (in parallel-connection) or a semi-transparent recombination layer consisting of an ETL and HTL (in series-connection) is required to connect the two sub-cells.

Owing to the lack of a printed semi-transparent electrode, highly efficient parallel-connected tandem devices are more difficult to realize than the series-connected ones.[17,36,37] Recently, several solution-processed semi-transparent electrodes, such as highly conductive poly(3,4-ethylenedioxythiophene):poly-(styrenesulfonate) (PEDOT:PSS)[38,39] and silver-nanowires (AgNWs),[40–42] have been reported to substitute ITO, exhibiting promising electrical and optical properties.

Different to the parallel-connected tandem device, the intermediate layer of the series-connected tandem device

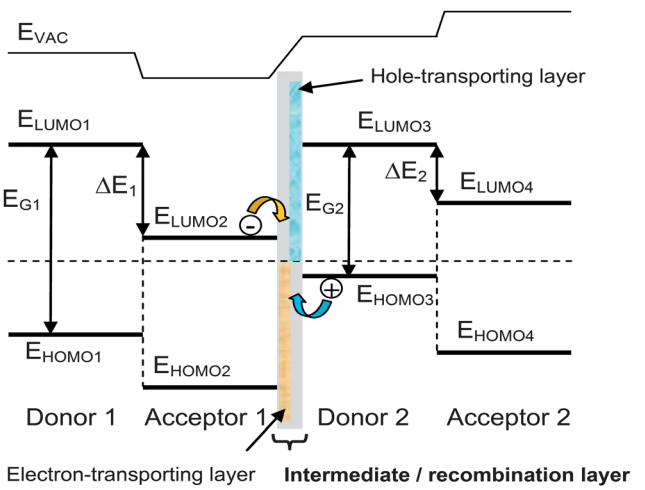

Fig. 7 Simplified band diagram of a tandem cell made of two sub-cells connected in series *via* a recombination layer.

functions as a recombination layer between the electrons and holes selectively collected from different sub-cells. In this case, the energetic diagram of the device can be represented as in Fig. 7. When compared to the complex semi-transparent electrode for the parallel-connected device, the solution-processed recombination layer for the series-connected device is straightforward to engineer under the following requirements:

- The intermediate layer should be highly transparent to minimize the optical losses.

- A quasi-ohmic-contact should be formed between the ETL and HTL to ease bipolar recombination.

- The recombination of the charge carriers in the IML needs to be balanced to maximize the short circuit current.

- The processing of the intermediate layer should match the requirements for mass production, *i.e.* solution-processing, low-temperature treatment, thickness requirement, *etc.*

- The intermediate layer should be robust enough to protect the underlying active layer from damage during processing of the upper layers.

- The intermediate layer should be environmentally stable to enhance the reliability and lifetime of the tandem device.

- The optical spacer effect of the intermediate layer on the light propagation inside the tandem device should be considered for further optimization.

In the past several years multiple efficient intermediate layers were developed for organic tandem solar cells.[17] Due to the lack of conductivity ultra-thin thermally evaporated metal layers were frequently evaporated between ETL and HTL to form an equivalent ohmic contact. An intermediate layer with non-ohmic contact properties typically has s-shaped *J–V* characteristics.[43–50] To overcome all these issues we demonstrated an easy but generic approach consisting of a solution-processed thin layer based Ag nanostructure to remove the recombination restrictions at the interface between the ETL and HTL.[51]

However, to keep the tandem architecture as simple as possible, a directly formed ohmic contact between the ETL and HTL is preferred. Most fundamental solution-processed intermediate layers are based on combinations of metal oxides (ETL) with highly conductive PEDOT:PSS (HTL) like TiO_x/PEDOT:PSS (PH500),[52,53] ZnO/PEDOT:PSS (PH500),[54] Orgacon[55,56] or Clevios F CPP105D[57]), *etc.* In these combinations the highly conductive PEDOT:PSS plays a crucial role in forming the quasi-ohmic contact. We have reported on an efficient intermediate layer consisting of aluminum doped ZnO (AZO) and low conductive PEDOT:PSS Al4083.[58] Due to the electrical properties of AZO *versus* ZnO, the quasi-ohmic contact that formed between the ETL and HTL is not determined by the conductivity of PEDOT:PSS. Consequently, the thickness of this intermediate layer could be extended from ~50 to 160 nm without compromising the efficiency of the tandem device. Zhou *et al.*[59] demonstrated that ethoxylated polyethylenimine (PEIE) can be used to universally modify the work function of electrodes. PEIE was demonstrated to serve as an efficient intermediate layer with highly conductive PEDOT:PSS (PH1000), although the interface properties between PEIE and PEDOT:PSS were not well understood.[60]

In addition to its function as a recombination layer, the intermediate layer of a tandem device may have further functionality. One example is the optical spacer effect, improving the tandem device performance by adjustment of the electrical field distribution within each sub-cells' active layer. Using PEDOT:PSS Al4083/AZO as an IML, optical simulations suggested a slight tuning of the photon absorption, resulting in an enhancement of J_{sc} for P3HT:PCBM/Si-PCPDTBT:PCBM sub-cells as a function of the IML thickness. This effect was also confirmed through experimental results where, for a given thickness of the active layers, the J_{sc} of the tandem device increased from -7.24 to -7.68 mA cm^{-2} as the IML was increased from ~50 to 160 nm.[58] A different but also attractive approach was demonstrated by J. Yang *et al.*[61] who investigated plasmonic effects in an inverted tandem cell configuration by blending Au nanoparticles (NPs) with the intermediate layer. A 20% improvement in power conversion efficiency was suggested due to plasmonic near-field enhancement.

4 Optical simulations of the tandem solar cells

In order to fully exploit the efficiency potential of promising materials, the combinations of absorbers *versus* layer sequence have to be understood. In addition, even for donor materials with attractive absorption properties, suitable acceptor molecules have to be chosen to ensure balanced photogeneration. Moreover, the thicknesses of the top and the bottom sub-cells must be carefully optimized to match the photocurrent from each sub-cell. In this regard, optical simulations are frequently employed to exploit the ultimate efficiency potential for different material combinations of the materials as a function of layer thickness.

Optical simulations of tandem cells were carried out with different methodologies such as the Rigorous Coupled Wave Analysis (RCWA)[62–64] or the Transfer Matrix Formalism (TMF).[65–67] Using these methods, the number of absorbed photons in each layer is calculated by considering the reflection, the transmission, and the electric field distribution for periodic structures. A multilayer OSC can be treated in the simplest case as a one-dimensional system and the amplitude of the electromagnetic field vector is coherently calculated for all layers. Prior to the simulations, the complex refractive indices (n + ik) of all the layers have to be determined. The imaginary part of the complex index of refraction (k) is directly measured by UV-vis spectrometry and the real part (n) by variable angle spectroscopic ellipsometry (VASE).

All the aforementioned concepts were successfully demonstrated by Dennler *et al.*,[68] performing detailed optical simulations of tandem solar cells based on the following organic semiconductors: poly(3-hexylthiophene) (P3HT), poly[2,6-(4,4-bis-(2-ethylhexyl)-4*H*-cyclopenta[2,1-*b*;3,4-*b*′]dithiophene)-*alt*-4,7-(2,1,3-benzothiadiazole)] (PCPDTBT), 1-(3-methoxycarbonyl)-propyl-1-phenyl[6,6] C61 (PC60BM), and 1-(3-methoxycarbonyl)-propyl-1-phenyl[6,6] C71 (PC70BM). The structure of the tandem cells is depicted in Fig. 8a. A 8 nm thick TiO_x and 25 nm thick PEDOT:PSS were employed as the intermediate layers. For each active layer pair, the thickness of both the bottom (d_{bottom} between 0 and 300 nm) and the top (d_{top} between 0 and 600 nm)

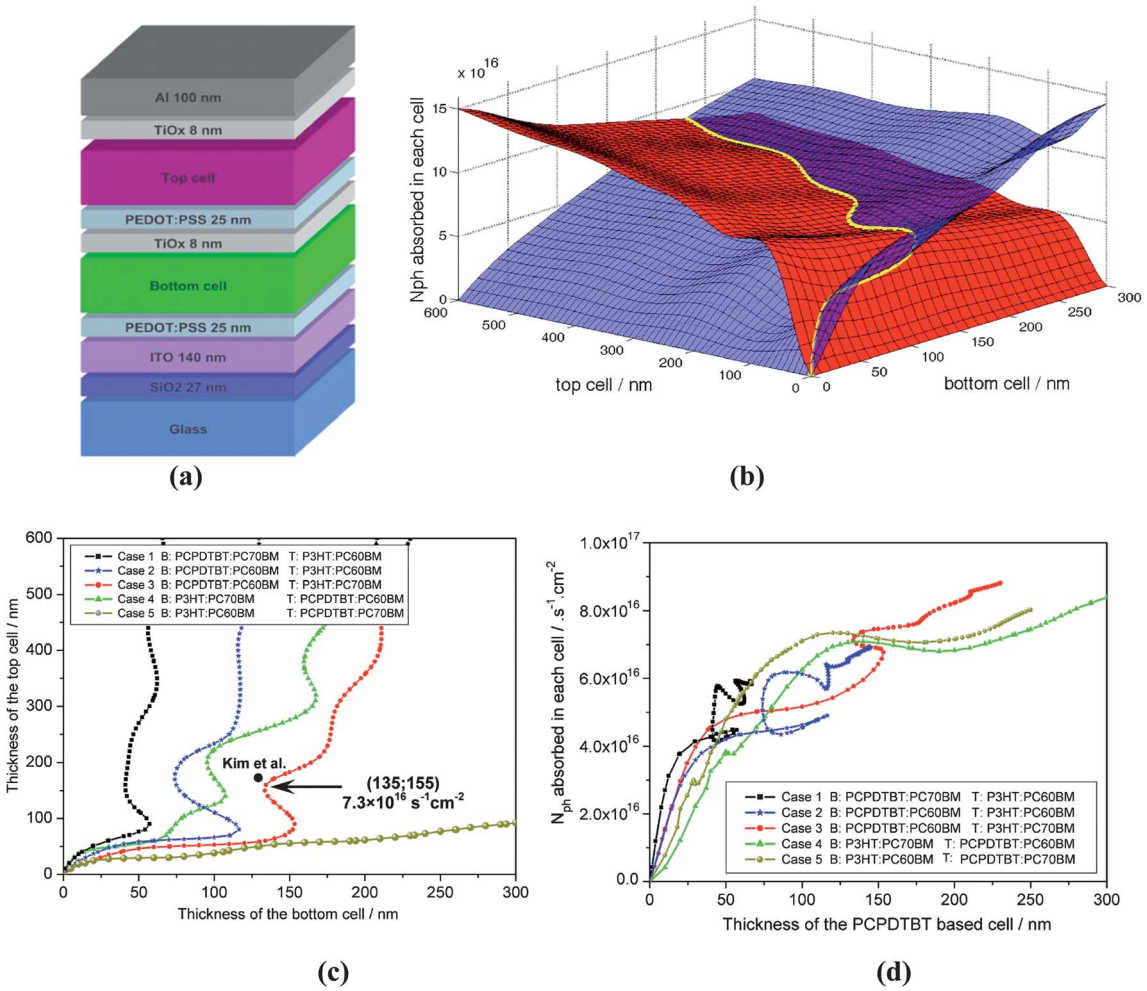

Fig. 8 (a) Schematic diagram of the structure of the tandem cells simulated by Dennler *et al.* for different material combinations as bottom and top sub-cells; (b) number of photons absorbed in the bottom active layer (blue surface) and in the top active layer (red surface) *vs.* the thickness of the bottom and the top active layers in a 3D plot. The yellow line indicates the isoline 1, where N_{ph}(bottom)/N_{ph} (top) = 1; (c) thickness relationship for reaching an equal number of photons absorbed in the top and the bottom cell, for each material combination; and (d) number of photons absorbed in both active layers (isoline 1) *vs.* the thickness of the PCPDTBT based active layer for various material combinations.[68] Reprinted with permission from ref. 68, Copyright 2007, American Institute of Physics.

active layers was varied and the number of photons absorbed (N_{ph}) in those layers under AM1.5G was calculated. An example of such a calculation with PCPDTBT:PC60BM as the bottom cell and P3HT:PC70BM as the top cell is shown in Fig. 8b. N_{ph} for the bottom [N_{ph} (bottom)] and the top [N_{ph} (top)] cells are represented in the three-dimensional space as surfaces, blue and red, respectively. The two surfaces N_{ph} (bottom) and N_{ph} (top) cross each other along a tortuous line defining the pair (d_{bottom}; d_{top}) for which N_{ph} (bottom) = N_{ph} (top). This line is called "isoline 1". The isoline 1 reports the optimum thicknesses of the active layers under the assumption that the top and bottom sub-cells have the same IQE and FF, independent of the active layer thickness. In contrast, the current of the whole tandem device would be optimized along another isoline for which N_{ph} (bottom)/N_{ph} (top) = const ≠ 1.

Fig. 8c shows the isoline 1 *versus* the thickness of the top and the bottom active layers for five different material combinations and layer sequences. This plot gives a quantitative understanding of the impact of layer design upon the tandem cell performance. Obviously, PCPDTBT:PC70BM for the bottom cell combined with P3HT:PC60BM for the bottom cell (case 1) and in *vice versa* sequence (case 5) have such different absorption properties that tuning of the active layers' thickness and achieving a balanced N_{ph} are very challenging. Replacing PC70BM by PC60BM in the bottom cell (case 2) allows one to utilize a thicker bottom cell compared to case 1. Interestingly, cases 3 and 4, using both the same blends but in a reversed layer sequence, show quite similar behavior with no obvious saturation for the thickness range investigated.

Valuable information can be deducted from the N_{ph}, plotted *versus* the thickness of the single layers as shown in Fig. 8d. This one displays the N_{ph} along the isoline 1 *versus* the thickness of the PCPDTBT based cell. This way of plotting was chosen because PCPDTBT cannot be processed in thick layers without losing its performance. As such, it is more critical to optimize the thickness of this cell. The optical interference effects cause quite unregularly shaped curves. N_{ph} for a single film thickness of the PCPDTBT layer can be matched by multiple layer

thicknesses of the P3HT layer. Specifically the case 3, whereas PCPDTBT:PC60BM is used as the bottom layer and P3HT:PC70BM as the top layer appears to be the most promising one for a reasonable thicknesses range of PCPDTBT between 130 and 230 nm. At these conditions the number of absorbed photons becomes maximized, which is reflected in higher current densities compared to the other scenarios. Despite intuition, the most efficient configuration puts the low bandgap polymer as the front absorber and the wide bandgap polymer as the back absorber. However, due to the specific optical absorption profiles of the two polymers and the thickness limitation of PCPDTBT, a configuration with the low bandgap polymer as the front or the bottom absorber allows higher performance as compared to other layer sequences.

Interestingly, Kim *et al.*[52] experimentally identified the same configuration as the most promising one. The diagram was approx. 135 nm PCPDTBT:PC60BM layer for the bottom sub-cell and 155 nm P3HT:PC70BM layer for the top sub-cell, resulting in efficiencies of 6.5%. However, beyond the fact that these results demonstrated excellent agreement between simulation and the experiment, it became very clear that the choice of the right acceptor plays a major role in the current balance of the tandem cells.

A direct comparison between the calculated photocurrent (based on optical simulations) and the experimental results allows identification of the current limiting sub-cell. For instance, according to the simulation results presented in Fig. 8, around 7.3×10^{16} photons per s per cm^2 are absorbed in each of the 135 nm thick PCPDTBT and 155 nm thick P3HT layers. Assuming an IQE of 100%, this N_{ph} would yield a short circuit current density of 11.7 mA cm^{-2}, while the current reported for this device is about 7.8 mA cm^{-2}. This indicates that the limiting sub-cell driving the J_{sc} in the tandem has an IQE of 67%, a value in good accordance with the IQE values which have been determined for PCPDTBT:PC60BM single devices. Hence this suggests that the performance of the device is limited by the PCPDTBT sub-cell for this combination.

5 Review of experimental results

From the very first organic tandem solar cell based on evaporated small molecules reported by Hiramoto *et al.* in 1990 (ref. 69) until the breakthrough of a 6.5% solution processed tandem cell reported by Kim *et al.* in 2007,[52] a detailed review of the reported organic multi-junction solar cells is presented in our previous work.[17] Since then, a growing number of records (around or higher than 5%) have been reported where the tandem/multi-junction structure improves the performance of the individual single sub-cells. Fabrication and reproducibility of highly efficient organic tandem solar cells have been reported to be very challenging. Currently, researchers have mainly focused on the exploration of novel materials which are suitable for tandem devices. In addition, new approaches on the design of intermediate layers, device structure and reliability of tandem solar cells have attracted considerable attention in recent years. In this section, the follow up and recent results of different types of organic tandem solar cells obtained by various groups are reviewed.

5.1 Highly efficient tandem organic solar cells based on novel materials

Recently, a great deal of effort is made to improve the power conversion efficiency of tandem OSCs based on novel materials including polymers as well as vacuum- and solution-processed small molecules. In the following, we present a review on highly efficient tandem solar cells based on both material categories.

5.1.1 Polymer based tandem organic solar cells. In 2010, Moet *et al.* reported a double junction device based on polyfluorene copolymer poly[9,9-didecanefluorene-*alt*-(bisthienylene) benzothiadiazole] (PF10TBT/PFTBT) and PCBM showing a power conversion efficiency of 4.5% achieved an efficiency enhancement of 13% compared to the single junction device.[70] They demonstrated that the optical and electrical losses of a only 80 nm single junction can be decoupled in a double junction solar cell to improve the efficiency.[71] For this tandem device fabricated in the normal architecture, a combination of a ZnO layer and PEDOT:PSS is served as the recombination layer. In order to keep the underlying ZnO layer intact, the acidity of the highly conductive PEDOT:PSS dispersion (Clevios PH500) was modified to a slightly basic pH 8.5 by addition of 3.0 vol% diluted 2-dimethylaminoethanol (DMAE, Aldrich) in water (ratio of 1 : 8 DMAE–H_2O). A direct consequence of the reduced work function of the neutralized PH500 is a V_{oc} reduction. Therefore, in the double junction solar cell an interfacial layer of Nafion was incorporated, by spin coating a perfluorinated Nafion resin solution, highly diluted in ethanol, on top of a modified PH500 anode before applying the second photoactive layer. The introduction of a thin layer of perfluorinated Nafion recovered the anode work function and gave a V_{oc} of 1.92 V for the tandem device. Although the achieved J_{sc} was just 3.49 mA cm^{-2}, the FF of 0.61 was considerable.

A very similar study was presented by Gilot and his colleagues.[72] In this case, the recombination layer consisted of 15 nm pH-neutral PEDOT:PSS spin-coated on a 30 nm ZnO layer, while the bottom and top sub-cells were based on a wide and a small band-gap polymer of PFTBT and poly[3,6-bis(4′-dodecyl-[2,2′]bithiophenyl-5-yl)-2,5-bis(2-ethylhexyl)-2,5-dihydropyrrolo[3,4-]pyrrole-1,4-dione] (pBBTDPP2) mixed with PCBM, respectively. Finally, for the tandem device composed of a 180 and a 120 nm thick bottom and top photoactive layer, an efficiency of 4.9% with $J_{sc} = 6.0$ mA cm^{-2}, $V_{oc} = 1.58$ V and FF = 0.52 was achieved. The V_{oc} equaled the sum of individual sub-cells' V_{oc} and demonstrated the functionality of their recombination layer. Notably, the J_{sc} of the tandem cell surpassed the lower current–density of the two sub-cells. The increased photocurrent generation in the bottom sub-cell originated from an increased electric field over this cell.[73] Holes extracted from the top sub-cell were not completely compensated for as fewer electrons from the bottom sub-cell did reach the recombination layer. At steady-state, this reduced the electric field across the top sub-cell and enhanced the effective field across the bottom sub-cell. Hence, at short-circuit conditions the top sub-cell operated in forward bias, whereas the bottom sub-cell experienced an equally large but opposite reverse bias, which assisted carrier collection in this layer. Especially for organic solar cells,

which generally exhibit a field assisted collection, this can be a significant effect.

The most efficient tandem cell comprising P3HT in both top and bottom photoactive layers was reported by Sakai *et al.* in 2010.[74] Two different kinds of fullerene derivatives were applied in the individual sub-cells, an 80 nm thick P3HT:bisPCBM cell showing high V_{oc} was employed as the top cell and a 200 nm thick P3HT:PC70BM cell showing high J_{sc} was employed as the bottom cell. Interestingly, they could achieve performance as high as 5.16%, which was enabled by their development of a deposition process employing a solvent blend in combination with a slow drying process without annealing.[75–77] In detail, P3HT:bisPCBM and P3HT:PC70BM were dissolved in a solvent blend of *o*-dichlorobenzene and chloroform at the ratio of 6 : 4. The recombination layer of indium tin oxide (ITO) sandwiched between MoO_3 and LiF was deposited by DC magnetron sputtering (ITO) and vacuum evaporation (LiF, MoO_3). A FF of 0.73, V_{oc} of 1.14 V and J_{sc} of 6.14 mA cm^{-2} were achieved for the best device in the normal structure. In particular, a FF of 0.73 is the highest value reported for OPV tandem cells fabricated so far. This high FF originated from the excellent carrier transport properties of both single cells as well as from the efficient charge carrier recombination at the designed interlayer.

Recently, Yang's group presented multiple reports on organic tandem solar cells. Chou *et al.* reported a 5.1% efficient inverted tandem solar cell applying a metal-oxide recombination layer in 2011.[78] The bottom and top sub-cells were prepared from P3HT:PCBM (150 nm) and poly[(4,4′-bis(2-ethylhexyl)-dithieno[3,2-*b*:2′,3′-*d*]silole)-2,6-diyl-*alt*-(2,1,3-benzothiadiazole)-4,7-diyl] (PSBTBT/Si-PCPDTBT) blended with PC70BM (120 nm), respectively. Among the different metal-oxide types tested, good performance was found for a combination of thermally evaporated MoO_3/sol–gel processed ZnO interlayers. An aluminum layer (1 nm by thermal evaporation) inserted between the MoO_3 and ZnO provided excellent electrical properties and good processability. Improving the intermediate layer, a V_{oc} of 1.2 eV, FF of 0.54 and J_{sc} of 7.84 mA cm^{-2} were achieved with an overall efficiency of 5.1%, which enhanced the highest single sub-cell's performance by over 25%. Previously, an efficiency of 5.84% was reported by the same group using more or less the same sub-cells, but instead a recombination layer of TiO_2/PEDOT:PSS and a conventional structure.[79] The J_{sc} of the inverted tandem cell was slightly higher than the value reported for the normal structure. Likely, the higher transmission of the metal oxide layers resulted in lower optical losses. As a result, the materials and configurations for the interlayer are no longer limited by the acidic PEDOT:PSS. Afterwards, Yang *et al.* suggested plasmonic effects in an inverted tandem solar cell by blending Au nanoparticles (NPs) with the recombination layer.[61] The respective tandem device was based on a bottom sub-cell of P3HT:indene-C60 bisadduct (ICBA) and a top sub-cell of PSBTBT:PC70BM. The Au NPs were blended with PEDOT:PSS/TiO_2:Cs and used as the recombination layer. The size of these Au NPs was estimated to be around 70–80 nm, which was comparable to the thickness of the deposited PEDOT:PSS layer. Therefore, it was anticipated that only a single layer of Au NPs was uniformly dispersed into the PEDOT:PSS matrix. Experimental results suggested that this plasmonic field enhancement improved both the top and bottom sub-cells' efficiency simultaneously by enhancing optical absorption. Efficiencies of 5.22 and 6.24% were reported for tandem solar cells without and with Au NPs in the recombination layer, respectively. The 6.24% efficient tandem cell including Ag NPs with V_{oc} = 1.45 V, FF = 0.61 and J_{sc} = 6.92 mA cm^{-2} improved the highest sub-cell's performance by around 30%. The plasmonic near-field intensification was further discussed by simulated near-field distribution and experimental Raman scattering investigation. This important effect was investigated earlier by Rand, Peumans and Forrest in 2004.[80] A normal structured tandem solar cell with 7% efficiency was achieved through modification of the inter-PEDOT:PSS layer.[53] The modified PEDOT (m-PEDOT:PSS) solution was made by mixing commercial PEDOT:PSS (PH500) with sodium polystyrene sulfonate (SPS). To further enhance the conductivity, 5% dimethylformamide (DMF), which is commonly used as a conductivity enhancer for PEDOT:PSS, was added to the m-PEDOT solution. This

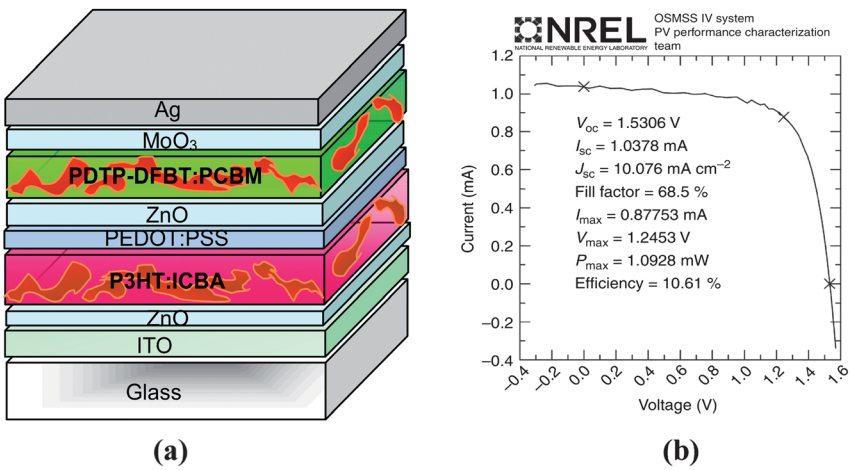

Fig. 9 (a) Schematic of the 10.6% efficient tandem solar cell demonstrated by You *et al.*;[92] (b) *J–V* characteristics of the device as measured by NREL under AM1.5G illumination (100 mW cm^{-2}). Reprinted with permission from ref. 92, Copyright 2013, Nature Publishing Group.

Table 1 Non-exhaustive survey of reports dealing with highly efficient tandem organic solar cells based on polymeric donors

		Bottom cell					Top cell					Tandem cell				
Year	Recombination layer	Active materials	V_{oc} (V)	FF	J_{sc} (mA cm^{-2}) (mW cm^{-2})	Eff. (%)	Active materials	V_{oc} (V)	FF	J_{sc} (mA cm^{-2}) (mW cm^{-2})	Eff. (%)	V_{oc} (V)	FF	J_{sc} (mA cm^{-2}) (mW cm^{-2})	Eff. (%)	Ref.
2007	8 nm TiO_x + 25 nm PEDOT:PSS	PCPDTBT:PCBM	0.66	0.5	9.2 (100)	3.0	P3HT:PCBM	0.63	0.69	10.8 (100)	4.7	1.24	0.67	7.8 (100)	6.5	52
2010	30 nm ZnO + 30 nm modified PH500 + thin layer of Nafion	PF10TBT:PCBM	0.98	0.66	5.6 (0.9)	4.0	PF10TBT:PCBM	0.98	0.66	5.6 (0.9)	4.0	1.92	0.61	3.49 (0.9)	4.5	71
2010	30 nm ZnO + 15 nm pH-neutral PEDOT:PSS	PFTBT:PCBM	0.98	0.52	5.5	—	pBBTDPP2:PCBM	0.61	0.57	6.2	—	1.58	0.52	6.0 (100)	4.9	72
2010	0.5 nm LiF + 20 nm ITO + 10 nm MoO_3	P3HT:bisPCBM	0.7	0.69	7.98 (100)	3.87	P3HT:PC70BM	0.58	0.64	11.3 (100)	4.21	1.14	0.73	6.14 (100)	5.16	74
2010	0.5 nm Al + 10 nm TiO_2 + 50 nm PEDOT:PSS	P3HT:PC70BM	0.6	0.66	9.27 (100)	3.77	PSBTBT:PC70BM	0.67	0.55	10.71 (100)	3.94	1.25	0.63	7.44 (100)	5.84	79
2011	10 nm MoO_3 + 1 nm Al + 30 nm ZnO	P3HT:PCBM	0.58	0.64	8.6 (100)	3.2	PSBTBT:PC70BM	0.64	0.49	11.7 (100)	3.7	1.20	0.54	7.84 (100)	5.1	78
2011	80 nm PEDOT:PSS (including Au NPs) + 10 nm TiO_2:Cs	P3HT:ICBA	0.83	0.64	7.95 (100)	4.25	PSBTBT:PC70BM	0.63	0.40	12.65 (100)	3.21	1.45	0.61	6.92 (100)	6.24	61
2011	20 nm TiO_2 + 90 nm modified PEDOT:PSS	P3HT:ICBA	0.82	0.65	8.5 (100)	4.5	PSBTBT:PC70BM	0.66	0.54	13.7 (100)	4.7	1.47	0.63	7.6 (100)	7.0	53
2012	30 nm ZnO + 20 nm PEDOT:PSS	PCDTBT:PC70BM	0.9	0.52	12.3 (100)	5.8	PDPP5T:PCBM	0.58	0.65	14.0 (100)	5.3	1.44	0.54	9.0 (100)	7.0	56
2012	40 nm PEDOT:PSS + 30 nm ZnO	P3HT:ICBA	0.82	0.65	7.48 (100)	4.4	PDPP5T:PCBM	0.59	0.67	13.31 (100)	5.0	1.35	0.6	7.23 (100)	5.8	89
2012	40 nm PEDOT:PSS PH1000 + 10 nm PEIE	P3HT:ICBA	0.82	0.63	8.8 (100)	4.5	PBDTTT-C:PCBM	0.67	0.57	15.2 (100)	5.9	1.5	0.72	7.7 (100)	8.2	60
2012	Modified PEDOT:PSS + ZnO	P3HT:ICBA	0.85	0.7	9.56 (100)	5.7	PBDTT-DPP:PC70BM	0.74	0.65	13.5 (100)	6.5	1.56	0.66	8.26 (100)	8.6	54
2012	30 nm PEDOT:PSS + 30 nm ZnO	P3HT:ICBA	0.84	0.7	9.5 (100)	5.6	PBDTT-SeDPP:PC70BM	0.69	0.62	16.8 (100)	7.2	1.52	0.66	9.44 (100)	9.5	91
2013	PEDOT:PSS + ZnO	P3HT:ICBA	0.84	0.71	10.3 (100)	6.1	PDTP-DFBT:PCBM	0.7	0.66	15.4 (100)	7.1	1.53	0.68	10.1 (100)	10.6	92

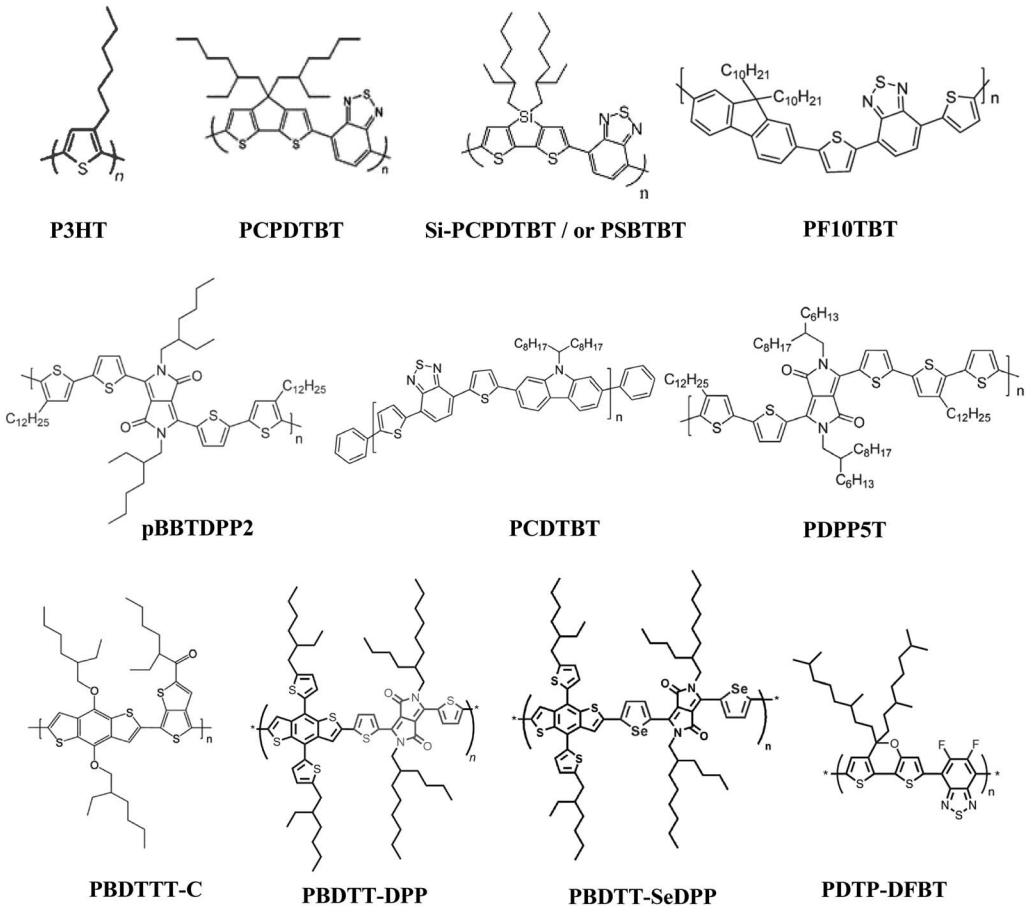

Fig. 10 Chemical structures of the most utilized donor materials in the tandem organic solar cells based on polymeric donors.

m-PEDOT:PSS inter-layer is physically robust enough to endure slow drying of solvents such as chlorobenzene (CB) and dichlorobenzene (DCB) during the top active layer deposition. The tandem device with final structure of ITO (150 nm)/PEDOT 4083 (40 nm)/P3HT:ICBA (150 nm)/TiO_2 (20 nm)/m-PEDOT (90 nm)/PSBTBT:PC70BM (100 nm)/Ca (20 nm)/Al (100 nm) achieved a high efficiency of 7% with V_{oc} = 1.47 V, J_{sc} = 7.6 mA cm^{-2}, and FF = 63%, under 100 mW cm^{-2} illumination of an AM1.5G solar simulator. Actually, in this tandem device a performance improvement of 30% was achieved *versus* the best single device (4.7% PSBTBT:PC70BM).

In 2012, Gevaerts *et al.*[56] reported efficiencies of over 7% for a normal structured tandem device. In this case, the large bandgap polymer of poly[*N*-9′-heptadecanyl-2,7-carbazole-*alt*-5,5-(4′,7′-di-2-thienyl-2′,1′,3′-benzothiadiazole)] (PCDTBT)[81–84] mixed with PC70BM and the novel low bandgap diketopyrrolopyrrole-quintetthiophene copolymer (PDPP5T)[85–88] blended with PCBM were employed as bottom and top sub-cells, respectively. Two different optimal layer thicknesses (80 and 210 nm) were identified, providing power conversion efficiencies of 5.6–5.8% for single PCDTBT:PC70BM cells. In these devices there is a trade-off between FF and J_{sc} while the V_{oc} is constant. The single cell of PDPP5T:PCBM with an optimized thickness of 120 nm led to efficiencies of 5.3%. Optical simulations, assuming a spectrally averaged IQE of 70% for PCDTBT:PC70BM and 76%

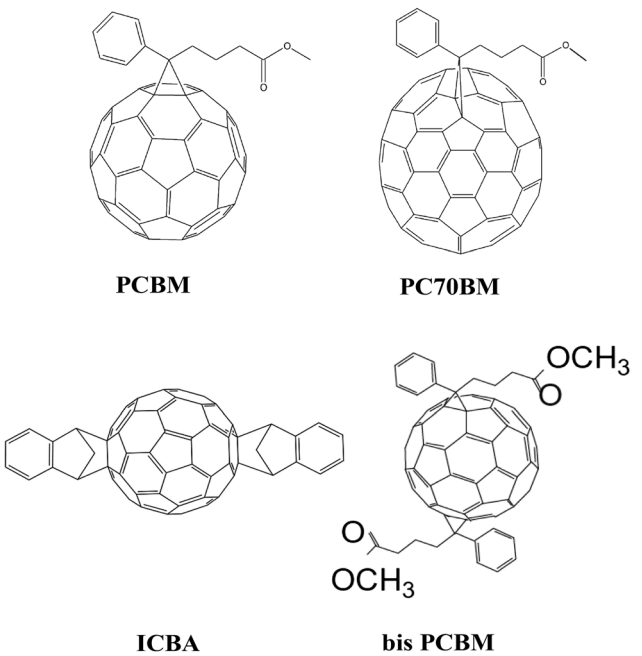

Fig. 11 Chemical structures of the most utilized acceptor materials in the tandem organic solar cells based on polymeric donors.

for PDPP5T:PCBM, predicted the maximum efficiency for a 170 nm PCDTBT:PC70BM bottom sub-cell combined with a 120 nm PDPP5T:PCBM top sub-cell. The intermediate layer consisted of a 30 nm thick layer of 4–5 nm ZnO nanoparticles and a 20 nm layer of pH neutral PEDOT:PSS. Experimentally, the authors demonstrated a 7.0% efficient tandem device with a V_{oc} of 1.44 V, FF of 0.54 and J_{sc} of 9 mA cm^{-2}. The experimental results closely match the optical prediction as well as calculated efficiency extracted from the reconstructed *J–V* characteristics of the tandem device. Reversing the device architecture and substituting the bottom sub-cell of PCDTBT:PC70BM with P3HT:ICBA, the efficiencies of 5.8% with V_{oc} = 1.35 V, FF = 0.6 and J_{sc} = 7.23 mA cm^{-2} were reported by the same group.[89] The solution-processed recombination layer consisted of 40 nm PEDOT:PSS and 30 nm ZnO nanoparticle layers. By using a mild N_2 plasma treatment and depositing PEDOT:PSS from water–isopropanol, followed by spin-coating ZnO nanoparticles, the authors were able to reproducibly create a recombination contact onto hydrophobic P3HT:ICBA layers. As an advantage of the inverted architecture, acidic PEDOT:PSS, which is known to easily dissolve ZnO, during PEDOT:PSS annealing does not cause a problem when ZnO nanoparticles are deposited on top of it.

Zhou *et al.*[60] reported on inverted polymer tandem solar cells wherein highly conductive PEDOT:PSS (PH1000) in combination with ethoxylated polyethylenimine (PEIE) acted as an efficient charge recombination layer. This surface modification with PEIE led to a high work function contrast between the two opposite interfaces of the charge recombination layer in contact with the bottom and top sub-cells in a tandem cell configuration where the sub-cells are connected in series. The bottom surface of the PEDOT:PSS displays a high work function of 4.9 eV, whereas the top surface modified by PEIE displays a low work function of 3.6 eV. A 200 nm thick P3HT:ICBA and 80 nm thick poly[(4,8-bis-(2-ethylhexyloxy)-benzo[1,2-*b*:4,5-*b*′]dithiophene)-2,6-diyl-*alt*-(4-(2-ethylhexanoyl)-thieno[3,4-*b*]thiophene)-2,6-diyl] (PBDTTT-C):PCBM blend were employed as the bottom and top photoactive layers, respectively. With this combination, tandem cells displayed excellent performance: V_{oc} = 1.48 V, J_{sc} = 7.4 mA cm^{-2}, FF = 0.68, and PCE = 7.5%, averaged over 25 devices, among which the champion cell showed V_{oc} = 1.5 V, J_{sc} = 7.7 mA cm^{-2}, FF = 0.68, and PCE = 8.2% under 100 mW cm^{-2} AM1.5 illumination. It is worthwhile mentioning that no post-treatment such as thermal annealing and/or UV illumination was required to activate the PEIE interface/intermediate layers.[90] The authors also tested PH1000/branched polyethylenimine (PEI) as the recombination layer in tandem solar cells. The cells with PH1000/PEI yielded very similar results to those of PH1000/PEIE. This is consistent with the fact that the reduction of the work function of PH1000 by coating PEIE or PEI is similar.[59]

In 2012, Yang's group reported the up to date most efficient polymer-based tandem solar cells. Dou *et al.*[54] demonstrated the rational design of a novel low-bandgap conjugated polymer, poly{2,6′-4,8-di(5-ethylhexylthienyl)benzo[1,2-*b*;3,4-*b*]-dithiophene-*alt*-5-dibutyloctyl-3,6-bis(5-bromothiophen-2-yl)-pyrrolo[3,4-*c*]pyrrole-1,4-dione} (PBDTT-DPP) with an optical bandgap of 1.44 eV for tandem solar cells. PBDTT-DPP blended with PC70BM gave PCEs greater than 6% for single cell devices in both normal and inverted structures. Among more than 300 devices processed, the best devices gave the following values: V_{oc} ≈ 0.74 V, J_{sc} ≈ 13.5 mA cm^{-2}, and FF ≈ 65%. The high V_{oc} can be attributed to the deep HOMO level of −5.3 eV and the high J_{sc} and FF can be attributed to the high hole mobility of PBDTT-DPP (the hole mobility of PBDTT-DPP:PC70BM with a 1 : 2 weight ratio was found to be 2.9 × 10^{-4} cm^2 V^{-1} s^{-1}). Finally, a PCE of 8.62% was certified by the National Renewable Energy Laboratory (NREL) for an inverted structure tandem solar cell comprised of P3HT:ICBA and PBDTT-DPP:PC70BM as the bottom and top sub-cells, respectively. A combination of m-PEDOT:PSS/ZnO ensured the efficient charge carriers recombination in the intermediate layer. The resulting tandem device showed a FF of 0.66, V_{oc} of 1.56 V, and J_{sc} of 8.26 mA cm^{-2}.

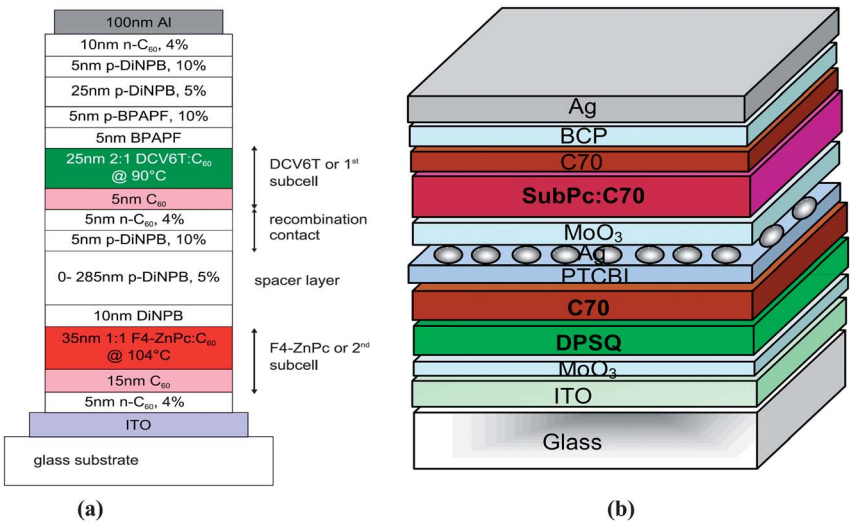

Fig. 12 Schematic of (a) a vacuum-processed small molecule based tandem solar cell demonstrated by Riede *et al.*[93] Reprinted with permission from ref. 93, Copyright 2011, Wiley-VCH. (b) A vacuum- and solution-processed small molecule based tandem solar cell demonstrated by Lassiter *et al.*[94]

Table 2 Non-exhaustive survey of reports dealing with highly efficient tandem organic solar cells based on small molecules

		Bottom cell				Top cell				Tandem cell				
Year	Recombination layer	Active materials	V_{oc} (V)	FF	J_{sc} (mA cm^{-2}) (mW cm^{-2})	Eff. (%)	Active materials	V_{oc} (V)	FF	J_{sc} (mA cm^{-2}) (mW cm^{-2})	Eff. (%)	V_{oc} (V)	FF	J_{sc} (mA cm^{-2}) (mW cm^{-2})	Eff. (%)	Ref.
2011	10 nm DiNPB + 165 nm *p*-DiNPB, 5% + 5 nm *p*-DiNPB, 10% + 5 nm *n*-C60, 4% + 5 nm C60	F4-ZnPc:C60	0.66	0.64	8.3 (100)	3.9	DCV6T:C60	0.88	0.66	8.3 (111)	4.3	1.59	0.61	6.18 (100)	6.07	93
2012	5 nm PTCBI + 0.1 nm Ag + 5 nm MoO_3	SubPc:C70	1.04	0.48	8.5 (100)	4.3	DPSQ/C70	0.94	0.71	6.1 (100)	4.1	1.97	0.54	6.2 (100)	6.6	94
2013	NR[a]	NR	NR	NR	NR	NR	NR	NR	NR	NR	NR	NR	NR	NR	12	97

[a] Not reported.

The substitution of S by Se on the DPP unit (PBDTT-SeDPP) led to a reduced bandgap (optical bandgap of 1.38 eV) and an enhanced hole mobility (6.9×10^{-4} cm^2 V^{-1} s^{-1}) compared to S-based PBDTT-DPP.[91] A higher photocurrent of 16.8 mA cm^{-2} and a PCE of 7.2% were obtained in a single junction of PBDTT-SeDPP:PC70BM. Even more importantly, this new Se-containing polymer significantly enhanced the tandem device performance up to 9.5%. Tandem PSCs with an inverted configuration were fabricated using PBDTT-SeDPP:PC70BM as the top sub-cell and P3HT:ICBA as the bottom sub-cell. The averaged PCE from 20 tandem devices was 9.5% with a V_{oc} of 1.52 V, a J_{sc} of 9.44 mA cm^{-2}, and a FF of 0.66. The V_{oc} of the tandem device is almost the sum of two sub-cells (0.84 V and 0.69 V), indicating the effectiveness of the high-performance IML of PEDOT:PSS/ZnO. The FF of the tandem device is around the average of the two sub-cells (70% for the bottom sub-cell and 62% for the top sub-cell). The major improvement compared to the previously reported tandem cells based on PBDTT-DPP is the J_{sc} (from 8.3 mA cm^{-2} to 9.4 mA cm^{-2}).

Finally, the efficiencies of 10.6% were achieved by the same group based on a developed structure of the reported low bandgap polymer of PCPDTBT.[92] First, a significantly enhanced V_{oc} was obtained by introducing two strong electron-withdrawing fluorine atoms on the benzothiadiazole (BT) unit, forming the difluorobenzothiadiazole (DFBT) unit to lower the HOMO level. Second, the bandgap was further decreased by inserting a strong electron-donating oxygen atom into the cyclopentadithiophene (CPDT) unit, creating the dithienopyran (DTP) unit. These two strategies led to the novel polymer poly[2,7-(5,5-bis-(3,7-dimethyl octyl)-5*H*-dithieno[3,2-*b*:20,30-*d*]-pyran)-*alt*-4,7-(5,6-difluoro-2,1,3-benzothiadiazole)] (PDTP-DFBT) with a bandgap of 1.38 eV, which also showed a high hole mobility (3.2×10^{-3} cm^2 V^{-1} s^{-1}) and deep HOMO level (−5.26 eV). Single junction devices based on PDTP-DFBT showed a high quantum efficiency of >60% from 710 to 820 nm and the spectral response extends to 900 nm. This led to a PCE of 7.1 and 7.9% when blended with PCBM and PC70BM, respectively. Tandem devices based on the bottom sub-cell of P3HT:ICBA and the top sub-cell of PDTP-DFBT:PCBM obtained the certified PCEs of 10.6% with a J_{sc} of 10.1 mA cm^{-2}, FF of 68.5% and V_{oc} of 1.53 V under standard reporting conditions (25 °C, 100 mW cm^{-2}, AM1.5G). The device structure is ITO/ZnO/P3HT:ICBA (220 nm)/PEDOT:PSS/ZnO/PDTP-DFBT:PCBM (100 nm)/MoO_3/Ag (Fig. 9a). The *J*–*V* characteristics of this tandem device, certified by NREL, are shown in Fig. 9b. The efficiency of 10.6% ranks the world's top level among polymer photovoltaic cells that are available at the moment.

A brief summary of the reports dealing with highly efficient tandem organic solar cells based on polymeric donors and their corresponding single sub-cells is presented in Table 1. Fig. 10 and 11 depict the chemical structures of the most commonly utilized donor and acceptor materials in those tandem devices, respectively.

5.1.2 Small molecule based tandem organic solar cells. Recently, Riede *et al.* presented a certified efficiency of 6.07% for a small molecule based tandem solar cell.[93] The absorption-complementary materials of fluorinated zinc phthalocyanine

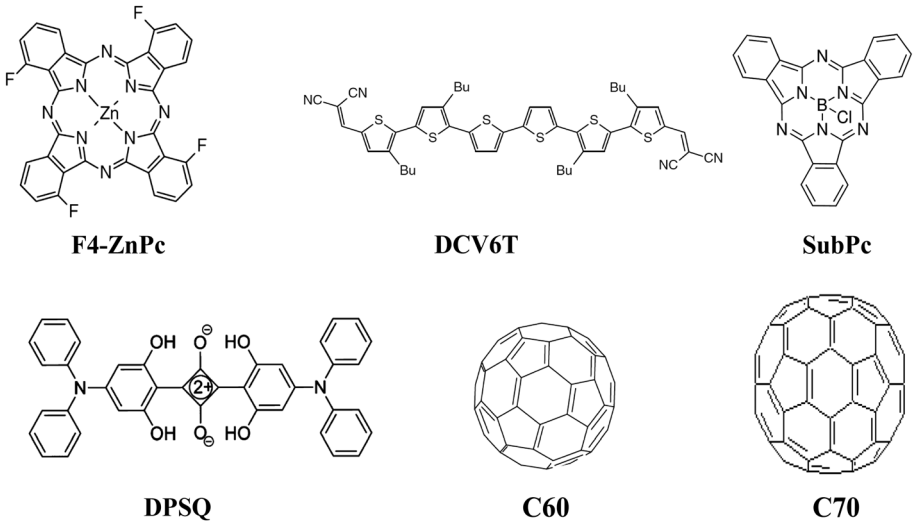

Fig. 13 Chemical structures of the most utilized materials in the tandem organic solar cells based on small molecules.

derivative (F4-ZnPc) and dicyanovinyl-capped sexithiophene derivative (DCV6T) blended with C60 were evaporated as bottom and top active layers, respectively. As shown in Fig. 12a, a complicated intermediate layer of *N*,*N*′-diphenyl-*N*,*N*′-bis(4′-(*N*,*N*-bis(naphth-1-yl)-amino)-biphenyl-4-yl)-benzidine (DiNPB), 5% p-doped DiNPB (p-DiNPB), 10% p-DiNPB, 4% n-doped C60 (n-C60), and C60 ensured the recombination of holes and electrons extracted from the bottom and top sub-cells. Thickness variations of the transparent optical spacer p-DiNPB between both sub-cells in the tandem solar cell were shown to cause a significant change in short circuit current density J_{sc} due to optical interference effects, whereas V_{oc} and fill factor were hardly affected. The maximum efficiency of about 6.07% under standard test conditions on a module relevant area of nearly 2 cm^2 with $V_{oc} = 1.59$ V, FF = 0.61 and $J_{sc} = 6.18$ mA cm^{-2} was reported for a spacer thickness of 150–165 nm.

Lassiter *et al.*[94] demonstrated a tandem organic photovoltaic cell incorporating solution- and vacuum-deposited small molecules as the active layers. In that work, the authors incorporated a solution-processed and solvent-vapor-annealed 2,4-bis[4-(*N*,*N*-diphenylamino)-2,6-dihydroxyphenyl] squaraine[95] (DPSQ)/C70 bilayer HJ for the bottom sub-cell and a boron subphthalocyanine chloride (SubPc):C70 graded HJ[96] for the top sub-cell. The tandem devices were fabricated with the following layer thicknesses: glass substrate/100 nm ITO/20 nm MoO_3/13 nm DPSQ/10 nm C70/5 nm PTCBI/0.1 nm Ag/5 nm MoO_3/29 nm SubPc:C70/3 nm C70/7 nm BCP/100 nm Ag (depicted in Fig. 12b). The intermediate layer consisting of PTCBI/Ag/MoO_3 was vacuum-processed. The resulting tandem device was demonstrated with a PCE of 6.66%, FF = 0.54, $J_{sc} = 6.2$ mA cm^{-2} and $V_{oc} = 1.97$ V, indicating a nearly loss free intermediate layer. The obtained efficiency for the tandem devices was at least 35% improved as compared to the most efficient single cell.

Recently, a new record of 12% on vacuum-processed organic tandem solar cells has been reported by Heliatek GmbH.[97] With Yang's group and Heliatek's new record-breaking efficiencies for organic photovoltaic cells,[92,97] the organics are now matching the a-Si:H. Unfortunately, no technical details on this record-efficient tandem solar cell have been reported so far.

A summary of the small molecule based tandem solar cells and their corresponding single sub-cells is provided in Table 2. The chemical structures of small molecules are shown in Fig. 13.

5.2 Highly efficient tandem organic solar cells based on various structures

In addition to the novel organic materials, various device architectures have been applied to enhance the efficiencies of tandem OPVs. A review of these structures including inorganic/organic hybrid, three-terminal and semi-transparent tandem organic solar cells is presented in the following.

5.2.1 Inorganic/organic hybrid tandem solar cells. In 2012, Seo and his colleagues[98] reported the record efficiency of inorganic/organic hybrid tandem solar cells. Fig. 14 shows the device structure of the inorganic/organic hybrid tandem solar cells designed in their work. Thin films of a-Si (p-type/intrinsic/n-type) were deposited as the bottom inorganic sub-cell using plasma enhanced chemical vapor deposition. The active layer of

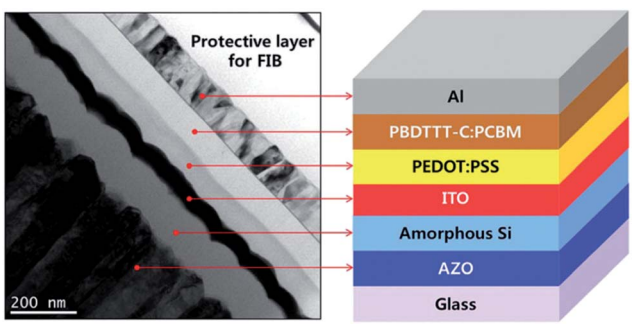

Fig. 14 High-resolution TEM cross-sectional image and the corresponding device structure of the hybrid tandem solar cell reported by Seo *et al.*[98] Reprinted with permission from ref. 98, Copyright 2012, Wiley-VCH.

Table 3 Non-exhaustive survey of reports dealing with highly efficient tandem organic solar cells based on hybrid and three-terminal structures

		Bottom cell					Top cell					Tandem cell				
Year (structure)	Recombination layer	Active materials	V_{oc} (V)	FF	J_{sc} (mA cm^{-2}) (mW cm^{-2})	Eff. (%)	Active materials	V_{oc} (V)	FF	J_{sc} (mA cm^{-2}) (mW cm^{-2})	Eff. (%)	V_{oc} (V)	FF	J_{sc} (mA cm^{-2}) (mW cm^{-2})	Eff. (%)	Ref.
2012 (hybrid)	50 nm ITO + 70 nm PEDOT:PSS	a-Si	0.8	0.64	7.86 (100)	4.11	PBDTTT-C:PCBM	0.75	0.53	11.54 (100)	4.65	1.42	0.58	6.84 (100)	5.72	98
2010 (three-terminal, common-anode)	PEDOT:PSS + 12 nm Au/5 nm V_2O_5	P3HT:PC70BM	0.58	0.60	10.1 (100)	3.5	PSBTBT:PC70BM	0.62	0.39	5.2 (100)	1.3	0.6	0.52	15.1 (100)	4.8	99

the organic top sub-cell consisted of a blend of PBDTTT-C:PCBM. The organic and inorganic solar cells were connected by a transparent ITO layer (50 nm) and a highly conductive PEDOT:PSS layer (70 nm). The ITO, acting as an electron transport layer, was deposited using magnetron sputtering. The PEDOT:PSS layer was used as the hole transport layer. Consequently, electrons extracted from the inorganic solar cells combined with holes extracted from the organic solar cells at the ITO/PEDOT:PSS interface. The maximum PCE of 5.72% with a V_{oc} of 1.42 V, J_{sc} of 6.84 mA cm^{-2} and FF of 0.58 was achieved, which is higher than that of either of the two sub-cells individually. The V_{oc} of the hybrid cell was 1.42 V, reaching 92% of the sum of the sub-cell V_{oc} values. This provided evidence that the two sub-cells were indeed connected in series. A brief summary dealing with this hybrid device and its corresponding single sub-cells is represented in Table 3.

5.2.2 Three-terminal tandem organic solar cells. A very different approach of Yang's group investigated three-terminal tandem devices (parallel connection of the sub-cells) based on the common-anode and common-cathode configuration.[99] In this configuration, the two sub-cells can be characterized individually as well as connected in parallel. In the case of a common-anode configuration, the bottom sub-cell of P3HT:PC70BM was made in the inverted structure and the top sub-cell of PSBTBT:PC70BM was made in the normal structure. An intermediate layer of PEDOT:PSS/12 nm evaporated Au/5 nm V_2O_5 formed the parallel connection. In contrast, the common-cathode configuration used a normal bottom sub-cell and an inverted top sub-cell separated by an intermediate layer of 15 nm TiO_2:Cs/3 nm evaporated Al/20 nm evaporated Au/TiO_2:Cs. The structures of the three-terminal devices based on both configurations are presented in Fig. 15. Although a 12 nm thick Au layer is sufficiently conductive to act as the third terminal, a thicker Au layer was used in the common-cathode configuration compared to the layer used in the common-anode configuration in order to compensate for the surface roughness of the TiO_2:Cs layer. The resulting tandem cell in the common-anode configuration showed a J_{sc} of 15.1 mA cm^{-2}, V_{oc} of 0.60 V, and FF of 0.52, resulting in a PCE of 4.8%. The tandem device J_{sc} which equaled the sum of the individual sub-cells' J_{sc} implied that the interlayer serves efficiently in collecting holes from the bottom and top sub-cells without any resistance losses. However, the common-cathode cells exhibited an overall PCE of 2.0% with a J_{sc} of 7.69 mA cm^{-2}, V_{oc} of 0.50 V, and FF of 0.52, which was ascribed to two main reasons. Firstly, the strong reflection of Au at near-IR wavelengths leads to a dramatic reduction in absorption of the top sub-cell, resulting in a very low J_{sc} (2.3 mA cm^{-2}). Secondly, deposition of thicker Au films leads to more pronounced Au diffusion and hence a small shunt resistance of the bottom sub-cell, leading to a low FF.

A brief summary dealing with the three-terminal device based on the common-anode configuration and its corresponding single sub-cells is represented in Table 3.

5.2.3 Semi-transparent tandem organic solar cells. Tang *et al.*[100] addressed the optical losses in a semi-transparent (ST) organic solar cell compared to the standard opaque one. In this work, an amphiphilic conjugated polymer poly(3,3′-([[(9′,9′-dioctyl-9*H*,9′*H*-[2,2′-bifluorene]-9,9-diyl)bis(4,1-phenylene)]bis(oxy))bis(*N*,

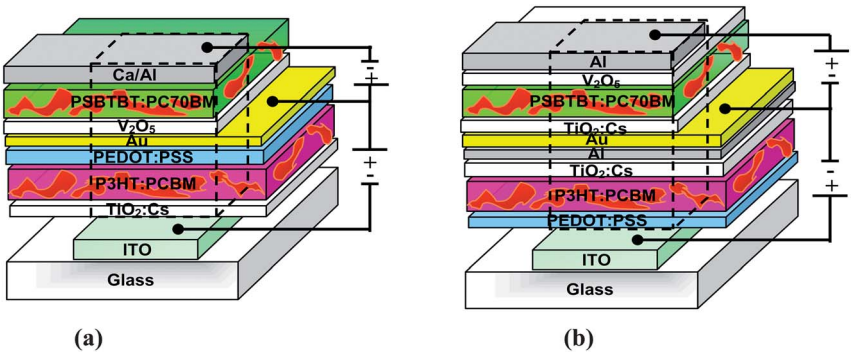

Fig. 15 Schematic of the three-terminal devices in the common-anode configuration (a) and common-cathode configuration (b) presented by Sista *et al.*[99] Reprinted with permission from ref. 99, Copyright 2010, Wiley-VCH. The dotted squares on the three electrodes denote the effective overlap areas for the two sub-cells.

N-dimethylpropan-1-amine)) (PFPA-1) modified ITO coated glass substrate and highly conductive PEDOT:PSS PH1000 were employed as the hole-collecting anode and ohmic electron-collecting cathode, respectively (Fig. 16a). The ST solar cells based on 90 nm thick poly[*N*,*N*′-bis(2-hexyldecyl)isoindigo-6,6′-diyl-*alt*-thiophene-2,5-diyl] (P3TI) and 80 nm thick poly[2,3-bis-(3-octyloxyphenyl)quinoxaline-5,8-diyl-*alt*-thiophene-2,5-diyl] (TQ1) mixed with PC70BM had remarkably high internal quantum efficiency at short circuit condition (~90%) and high transmittance (~50%). The ST tandem solar cells based on the same absorbing material as well as different absorbing materials were constructed in both parallel and series configurations by connecting the stacked two ST sub-cells externally. The representative solar cell performance parameters of those ST tandem solar cells as well as their corresponding individual sub-cells are listed in Table 4. When the sub-cells were connected in parallel, PCEs of 5.22%, 3.98%, and 4.52% could be obtained from the ST tandem solar cells with both sub-cells based on respectively P3TI:PC70BM, TQ1:PC70BM, and the ST tandem cell with a bottom sub-cell based on TQ1:PC70BM and a top sub-cell based on P3TI:PC70BM. A decent transmittance of ~25% was obtained from these ST tandem solar cells. The PCEs obtained from the series ST tandem solar cells were generally lower than those from the parallel tandem solar cells, due to imbalanced J_{sc} generated in the bottom and the top sub-cell. However, the FF was much higher in the series tandem solar cells than in the parallel tandem solar cells, obviously due to the fact that the characteristic resistance ($R_{CH} = V_{oc}/J_{sc}$)[100–102] was significantly larger in series configuration. Eventually, with a better J_{sc} matching achieved the difference in PCE between the series and parallel configuration would become smaller. In this case, the efficiencies of 4.52% (with FF = 0.62, V_{oc} = 0.73 V and J_{sc} = 9.95 mA cm^{-2}) and 4.35% (with FF = 0.67, V_{oc} = 1.46 V and J_{sc} = 4.47 mA cm^{-2}) were achieved for the parallel and series configurations, respectively. These ST tandem devices showed ~15 % and ~23% performance losses for parallel and series configurations, respectively, compared to opaque operation with a reflective aluminum mirror behind the ST tandem cells. Moreover, the PCEs of 6.6% and 5.31% were predicted for the ST tandem solar cells with five sub-cells of P3TI:PC70BM and TQ1:PC70BM, respectively, connected in parallel.

The chemical structures of P3TI and TQ1 are shown in Fig. 16b.

5.3 Novel approach on intermediate layer

As a novel approach, applications of CVD grown graphene[103] as well as solution-processed graphene oxide[104] in the intermediate layer of organic tandem solar cells were reported in 2011.

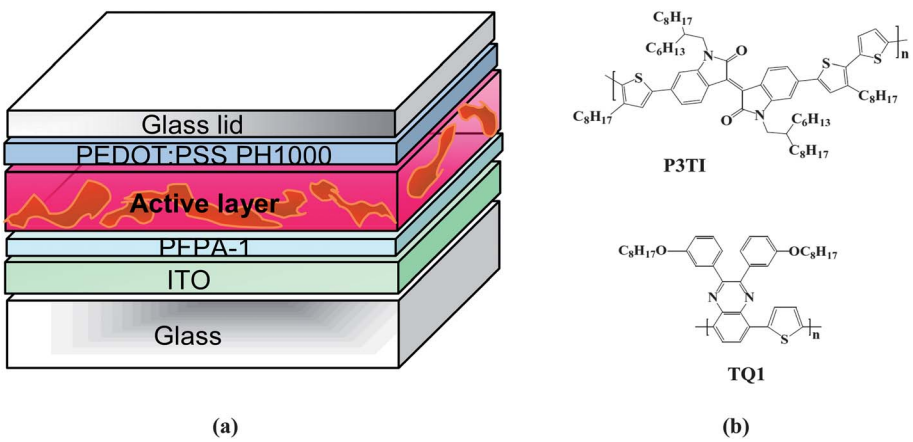

Fig. 16 (a) Schematic of the semitransparent single junction solar cells reported by Tang *et al.*[100] and (b) chemical structures of the utilized materials in the semitransparent solar cells.

Table 4 Representative solar cell performance parameters of the ST tandem solar cells and corresponding individual sub-cells reported by Tang *et al.*[100] The ST tandem devices have been constructed in both parallel and series configurations by connecting the stacked two ST sub-cells externally

Bottom sub-cell					Top sub-cell					Tandem cell				
Active materials	V_{oc} (V)	FF	J_{sc} (mA cm^{-2}) (mW cm^{-2})	Eff. (%)	Active materials	V_{oc} (V)	FF	J_{sc} (mA cm^{-2}) (mW cm^{-2})	Eff. (%)	Configuration[a]	V_{oc} (V)	FF	J_{sc} (mA cm^{-2}) (mW cm^{-2})	Eff. (%)
P3TI:PC70BM	0.71	0.6	8.39 (100)	3.57	P3TI:PC70BM	0.68	0.63	4.04 (100)	1.73	P	0.69	0.61	12.4 (100)	5.22
										S	1.4	0.67	4.22 (100)	3.96
TQ1:PC70BM	0.77	0.62	5.72 (100)	2.75	TQ1:PC70BM	0.75	0.66	2.8 (100)	1.38	P	0.76	0.62	8.45 (100)	3.98
										S	1.52	0.67	2.96 (100)	3.02
TQ1:PC70BM	0.78	0.62	5.7 (100)	2.77	P3TI:PC70BM	0.69	0.63	4.3 (100)	1.87	P	0.73	0.62	9.95 (100)	4.52
										S	1.46	0.67	4.47 (100)	4.35
TQ1:PC70BM	0.78	0.62	6.21 (100)	3.0	P3TI:PC70BM	0.69	0.63	5.94 (100)	2.58	P, O	0.73	0.6	12.08 (100)	5.29
										S, O	1.46	0.64	6.03 (100)	5.63

[a] P = parallel, S = series, O = opaque.

Although the unique electronic and mechanical properties of graphene suggested numerous applications, the large-scale direct synthesis and solution-based handling were proven difficult. It has been suggested that a functionalized form of graphene, namely graphene oxide (GO), could provide a solution-friendly route to facile, high-throughput graphene manipulation. GO can be viewed as a two dimensional, random diblock copolymer with distributed nanosized graphitic patches and highly oxidized domains, thus capable of guiding the assembly of other materials through both π–π stacking and hydrogen bonding. Tung *et al.*[104] prepared GO by a modification of Hummers' method[105] and mixed it with the conducting PEDOT:PSS in water to obtain a dispersion with dramatically increased viscosity which turns into sticky thin films upon casting. The GO/PEDOT gel was functioning as a metal-free intermediate layer in a P3HT:PCBM based tandem solar cell by a direct adhesive lamination process. Fig. 17 shows the architecture of the device after each step of fabrication. First, the P3HT:PCBM active layer (130 nm) of the top (rear) sub-cell was spin-cast onto a polydimethylsiloxane (PDMS) stamp. A GO/PEDOT layer (10 nm) was then spin-coated on top of this active layer from an aqueous dispersion. In parallel, a bottom (front) sub-cell was fabricated by spin-coating P3HT:PCBM (150 nm) on a PEDOT:PSS modified indium tin oxide substrate. The bottom sub-cell was further coated with a layer of ZnO (~20 nm) as a part of the IML. Next, the two sub-cells were directly glued together and annealed at 150 °C. This annealing step further increased the electrical conductivity of the interconnection and improved the adhesion between the two sub-cells. Finally, the PDMS stamp is peeled off from the rear cell before depositing the top metal electrode. The V_{oc} of the tandem cell was 0.94 V, reaching 84% of the sum of the sub-cell V_{oc}. The PCE of the final tandem cell is calculated to be 4.14%, which is higher than that of either of the two cells (2.92% and 3.75%, respectively).

Later, the authors were able to further modify the properties of the GO-based interfaces by adding a small amount of single-walled carbon nanotubes (SWCNTs) into GO, which did not affect their solution processability but improved the vertical

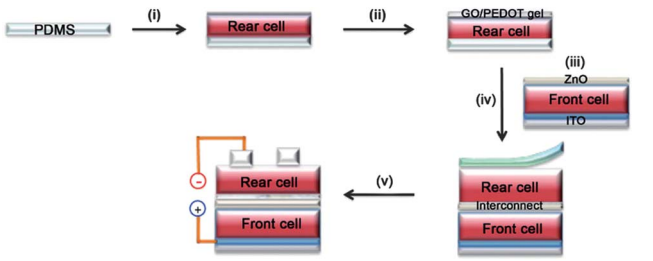

Fig. 17 Schematic diagram illustrating the construction of a tandem solar cell using the GO/PEDOT sticky interconnect. (i) The active layer of the top (rear) sub-cell is first spin-cast onto a PDMS stamp. (ii) GO/PEDOT gel is spin-coated on top of the active layer. (iii) A ZnO layer is spin-coated on top of a separately prepared bottom (front) sub-cell as a part of the IML. (iv) The top sub-cell is directly glued to the bottom sub-cell. Subsequential annealing at 150 °C can convert GO to the more conductive reduced GO and improve the adhesion between the two sub-cells. (v) Finally, the PDMS stamp is peeled off for thermal evaporation of the top metal electrodes.[104] Reprinted with permission from ref. 104, Copyright 2011, American Chemical Society.

Table 5 Non-exhaustive survey of reports dealing with highly efficient tandem organic solar cells based on the GO intermediate layer

		Bottom cell					Top cell					Tandem cell				
Year	Recombination layer	Active materials	V_{oc} (V)	FF	J_{sc} (mA cm^{-2}) (mW cm^{-2})	Eff. (%)	Active materials	V_{oc} (V)	FF	J_{sc} (mA cm^{-2}) (mW cm^{-2})	Eff. (%)	V_{oc} (V)	FF	J_{sc} (mA cm^{-2}) (mW cm^{-2})	Eff. (%)	Ref.
2011	20 nm ZnO + 10 nm GO/PEDOT:PSS	P3HT:PCBM	0.59	—	—	2.92	P3HT:PCBM	0.53	—	—	3.75	0.94	—	—	4.14	104
2012	ZnO + 3–4 nm GO/SWCNTs	P3HT:PCBM	0.56	0.59	9.39 (100)	3.41	P3HT:PCBM	—	—	—	—	0.94	0.58	7.4 (100)	4.1	107
2012	3–4 nm GO/SWCNTs + 30 nm ZnO	P3HT:PCBM	0.53	0.58	9.28 (100)	2.9	P3HT:PCBM	—	—	—	—	0.83	0.55	7.27 (100)	3.5	107

resistance of the resulting thin film. This allowed the use of thicker 3–4 nm GO thin films rather than *e.g.*, 1–2 monolayers.[106] In a rather similar fabrication procedure described in Fig. 17, GO–SWCNT composites in combination with ZnO were employed as the IML of P3HT:PCBM based tandem solar cells in an inverted as well as normal structure.[107] Average PCEs of 4.1% (with V_{oc} = 0.94 V, FF = 0.58 and J_{sc} = 7.4 mA cm^{-2}) and 3.5% (with V_{oc} = 0.83 V, FF = 0.55 and J_{sc} = 7.27 mA cm^{-2}) were achieved for the normal and inverted structure, respectively.

A summary of the reports dealing with tandem solar cells based on the GO intermediate layer is given in Table 5.

6 Tandem solar cell measurement

For a better insight into the working mechanisms of organic tandem solar cells and the accurate determination of the power conversion efficiency it is important to assess the performance of each individual sub-cell in a tandem device. By knowing the EQE of the sub-cells, it is possible to determine which of the sub-cells is limiting the performance. Nowadays, much effort is devoted to the development of multi-junction solar cells, for record efficiency, and hence, reporting the accurate performance has become an increasingly important subject for the OPV community. EQE measurements are essential to report precise PCEs of the tandem devices. Therefore, there is a strong need for a customized protocol to measure the EQE of these cells correctly. In contrast to single junction solar cells consisting of just one absorber layer, measuring the EQE for a tandem cell is significantly more challenging, especially for the technologically attractive two-terminal configuration where the intermediate contact is buried and sub-cells cannot be addressed individually. Although some detailed protocols for EQE measurement of two terminal tandem and triple junction inorganic solar cells were developed,[108–113] specific characteristics, such as a field-assisted charge collection and sub-linear light intensity dependence, limit their use for organic tandem solar cells. These properties necessitate that EQE experiments are carried out under representative illumination conditions and electrical bias to maintain short-circuit conditions for the addressed sub-cell.

A tandem cell is only able to pass current when both the wide and small bandgap sub-cells are simultaneously excited with light. Therefore, the EQE of organic tandem cells requires selective background illumination to optically bias one sub-cell such that the other sub-cell, which is under investigation, is current-limiting over the entire wavelength range.[114] Due to frequently observed sub-linear light intensity dependence of organic solar cells, the EQE under reduced light intensity, *e.g.* under monochromatized white light, is often overestimated compared to the response under standard operating conditions (AM1.5G with a light intensity of 100 mW cm^{-2}).[115] This consideration needs to be taken into account for EQE measurement, as explained in detail in the following.

In addition, under background illumination at short-circuit conditions the current-limiting sub-cell is actually operating under reverse bias because the optically biased sub-cell operates close to V_{oc}. This effect is illustrated in Fig. 18 for a 4.9% organic

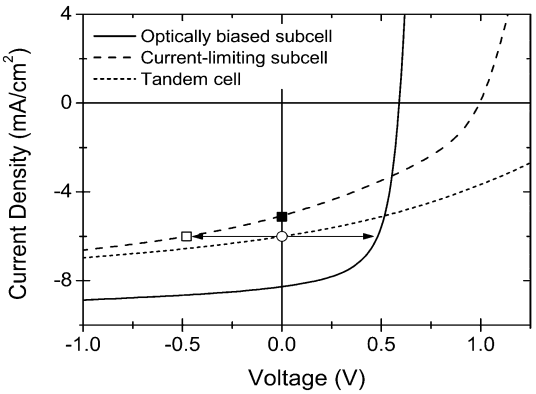

Fig. 18 Influence of the bias voltage of the optically biased sub-cell on the current-limiting sub-cell. ■ is the target value while □ is the obtained value when measuring the tandem cell under short-circuit conditions.[116] Reprinted with permission from ref. 116, Copyright 2010, Wiley-VCH.

tandem solar cell comprising wide and small bandgap polymers and a ZnO/PEDOT:PSS recombination layer.[116] Therefore, a forward bias voltage on the tandem cell is required to compensate for this effect and to avoid the overestimation of the EQE. The EQE overestimation depends on the magnitude of the slope of the *J*–*V* curve around $V = 0$ (*e.g.* in the example shown in Fig. 18, the error induced is about 16%).

Gilot *et al.* developed a method to determine the magnitudes of the background illumination and bias voltage during EQE measurements, based on the behavior of single junction cells and optical modeling.[116] Fig. 19a depicts a simplified schematic diagram of the EQE set-up presented in their work. It consists of a tungsten–halogen white light that is modulated with a mechanical chopper and then dispersed by a monochromator. Further two cw semiconductor lasers are used for bias illumination with wavelengths tuned to excite the photoactive layers in the different sub-cells. Their intensity can be varied with circular variable neutral density filters. A lock-in amplifier referenced to the mechanical chopper is used as a measuring unit. The device whose EQE measurement is presented here has been described previously[72] and is based on PFTBT as a wide bandgap polymer and pBBTDPP2 as a small bandgap polymer, both in combination with PCBM. The normalized absorption spectra of individual films of the active layers of the sub-cells are displayed in Fig. 19b and show the wavelengths used for the bias illumination. Since the PFTBT:PCBM layer is insensitive to light above 750 nm, bias illumination with a 780 nm laser is well suited to generate excess charges in the small bandgap top sub-cell and measure the current limiting wide bandgap bottom sub-cell in the tandem device. On the other hand, the low absorption of pBBTDPP2:PCBM in the 500 to 550 nm region enables selective excitation of the small bandgap top sub-cell in the EQE measurement of the tandem cell with bias illumination from a 532 nm laser.

To simulate the 1 sun operating conditions for each sub-cell, the following procedure was proposed by the authors; for the small bandgap top sub-cell, sufficient flood light is provided by the 532 nm bias illumination. This can be explained by considering that while the 532 nm light is primarily absorbed by the wide bandgap bottom sub-cell (creating the optical bias), also the small bandgap top sub-cell absorbs a substantial amount at this wavelength and the intensity of the 532 nm light can be tuned to generate 1 sun operating conditions in the small bandgap top sub-cell. In this regard, the appropriate AM1.5G equivalent intensity for 532 nm laser flood light was determined from the absorption profile of the tandem sub-cells obtained by calculating the number of absorbed photons using optical modeling. For the example described here, the authors had found that at this intensity and wavelength (532 nm), the wide bandgap bottom sub-cell absorbs *ca.* three times more light, which ensures that the small bandgap top sub-cell remains current-limiting. For the EQE measurement of the wide bandgap bottom sub-cell, the 780 nm laser light could only be used as bias light for the small bandgap top sub-cell, but could not act as flood light to have the wide bandgap bottom sub-cell operating under 1 sun conditions. Hence, the intensity of the 780 nm bias light was just tuned to AM1.5G equivalent intensity for the small bandgap single junction cell which ensures enough charge generation in the small bandgap top sub-cell, exceeding the charge generation in the wide bandgap bottom sub-cell at any wavelength of the modulated probe light. Afterwards, a mathematical correction of the measured EQE is

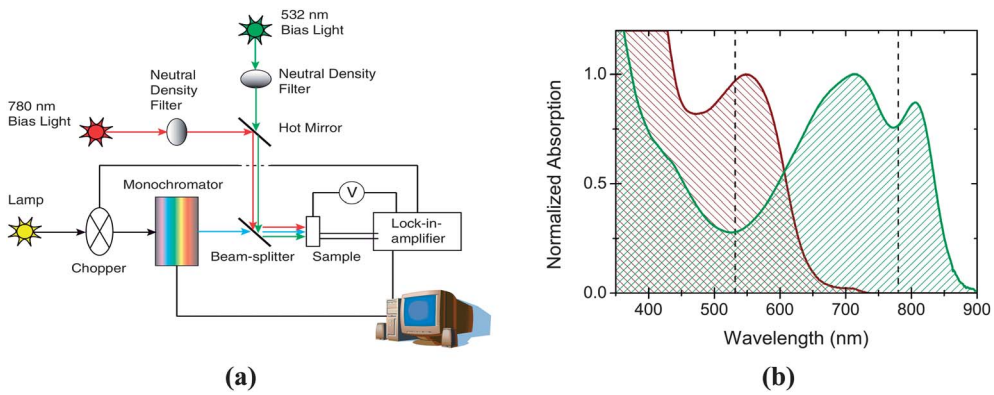

Fig. 19 (a) Set-up for the EQE measurement of tandem solar cells presented in ref. 116 and (b) normalized absorption spectra of both individual active layers (PFTBT:PCBM in wine and pBBTDPP2:PCBM in green). The dotted lines represent the wavelengths of the bias illumination.[116] Reprinted with permission from ref. 116, Copyright 2010, Wiley-VCH.

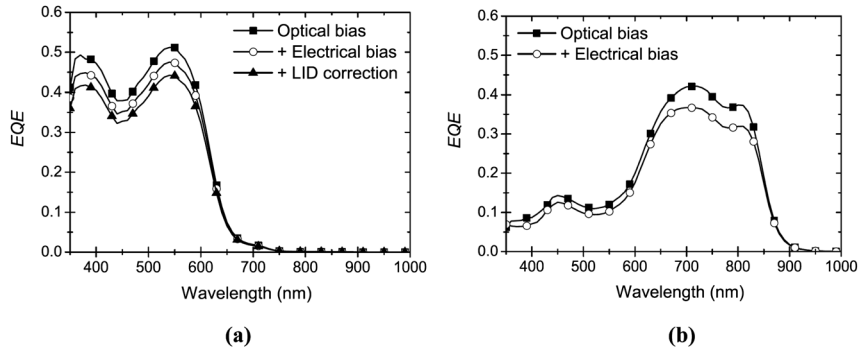

Fig. 20 The EQE of the (a) wide bandgap bottom sub-cell and (b) small bandgap top sub-cell after applying relevant optical and electrical biases. For the wide bandgap bottom sub-cell an extra light intensity dependence (LID) correction is required.[116] Reprinted with permission from ref. 116, Copyright 2010, Wiley-VCH.

applied to correct for the sub-linear light intensity dependence of the current. This correction factor is determined as the average ratio between the EQE measurements with and without 1 sun intensity flood light of a wide bandgap single junction device.

In the next step, the magnitude of the electrical bias was determined. The correct electrical bias could be determined by making use of the *J–V* characteristics of the single junction solar cells under illumination conditions representative for the sub-cells in the tandem device. The number of absorbed photons and subsequently J_{sc} was again calculated by optical modeling. However, during the EQE measurement, the tandem cell also experienced the modulated probe light on top of the bias illumination, generating additional current in the sub-cells. Since the variation of probe light intensity for different wavelengths caused a variable electrical bias, an average value of the electrical bias at wavelengths of minimal and maximal additional current generation of the modulated probe light could be applied. In this work the wavelengths of 350 nm and 550 nm, respectively, for the wide band gap bottom sub-cell and 350 nm and 800 nm for the small band gap top cell were selected. As a result, the average electrical bias needed for the EQE measurements was 0.60 and 0.90 V for the wide band gap front cell and the small band gap back cell, respectively.

As illustrated in Fig. 20, the applied optical and electrical bias influences the EQE of the sub-cells of the organic tandem solar cell significantly. This clearly demonstrates that careful determination of the magnitude of the optical and electrical bias is essential for accurate EQE measurements.

Finally, the calculated J_{sc} based on the sub-cells' EQE spectra and accordingly modified *J–V* characteristics of the single junction solar cells, representative of bottom and top sub-cells, can be used to construct the *J–V* characteristics of the tandem device.[72,116,117] The J_{sc} of a tandem device estimated *via* convolution of the EQE with the AM1.5G solar spectrum has shown a comparable result to that obtained with a class-A solar simulator. This demonstrates that the EQE was accurately determined with the protocol developed by Gilot *et al.* The same approach can be employed to measure the *J–V* characteristics of individual sub-cells in two-terminal organic tandem solar cells, where the EQE spectra of each sub-cell are obtained by varying the electrical bias over the tandem cell.[118] Integration of the resulting EQE with the AM1.5G solar spectrum for each value of *V* corresponds to measurement of the *J–V* characteristics of the sub-cells under a solar simulator. In an EQE measurement, indeed, the response of the cell to modulated light is measured, which means only the photocurrent (J_{photo}) is determined. Therefore, just the J_{photo}–*V* curve obtained from $J_{photo} = J_{light} - J_{dark}$ of a single reference cell measured under a solar simulator can be compared to the curve from the EQE measurement. However, the lower temperature in the dark measurement may cause an overestimation of J_{photo}.[118,119] To determine the V_{oc} of the sub-cells, the photocurrent curve can be summed with a measured dark curve of a single reference cell, identical to the sub-cell. It is worth mentioning that the long and intense illumination during the bias dependent EQE measurements may degrade the tandem cell, as observed by Gilot *et al.*[118]

7 Summary and outlook

Organic tandem solar cells have shown tremendous progress in recent years. As illustrated in Fig. 21, power conversion efficiencies over 10% were achieved. Although, vacuum-processed tandem solar cells have currently demonstrated higher record performance than solution-processed tandem solar cells, most efforts have been concentrated on the latter one. This explained

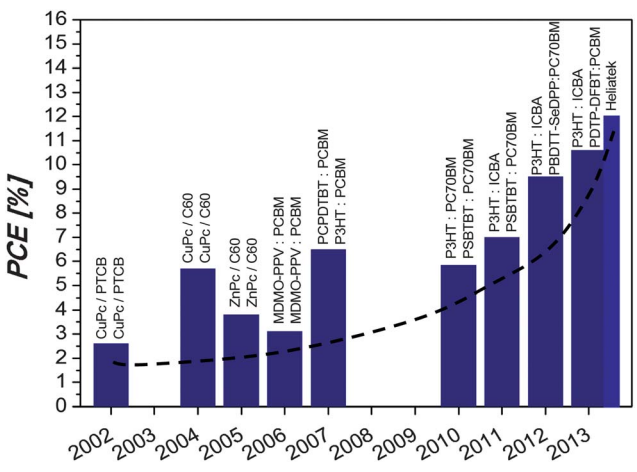

Fig. 21 Recent progress in power conversion efficiency of organic tandem solar cells.

the importance and attraction towards large area roll-to-roll printing of organic solar cells. According to the reports, the large bandgap sub-cell is dominantly based on P3HT, which is well known for its high crystallinity but also for its availability at reasonable quality and costs. As a big advantage, P3HT is exclusively functional with many different multi-adduct fullerene derivatives, leading to the higher V_{oc}. On the low bandgap absorber side, more work needs to be done with special importance on absorbers outreaching into the 900 nm region. Appropriate low bandgap couples need to be designed and synthesized based on the design rules for organic tandem solar cells. Understanding the detailed operation mechanisms of the device, designing novel high potential materials and improving the robustness of the intermediate layer will open the door to further enhance the efficiency of organic tandem solar cells beyond 15%.

Acknowledgements

The authors gratefully acknowledge the support of the Cluster of Excellence "Engineering of Advanced Materials" at the University of Erlangen-Nuremberg, which is funded by the German Research Foundation (DFG) within the framework of its "Excellence Initiative". T. Ameri thanks the Solar Technologies go Hybrid (SolTech) project for the financial support. N. Li acknowledges the financial support of the European Commission as part of the Framework 7 ICT 2009 collaborative project ROTROT ("roll to roll production of organic tandem cells", Grant no. 288565) project.

References

1 M. Z. Jacobson and G. M. Masters, *Science*, 2001, **293**, 1438.
2 S. Pacala and R. Socolow, *Science*, 2004, **305**, 968.
3 V. Fthenakis, J. E. Mason and K. Zweibel, *Energy Policy*, 2009, **37**, 387.
4 M. Z. Jacobson and M. A. Delucchi, *A path to sustainable energy by 2030*, Scientific American, November 2009.
5 R. Perez and M. Perez, A fundamental look at energy reserves for the planet, *The IEA SHC Solar Update*, 2009, vol. 50, p. 2.
6 A. Jäger-Waldau, F. Monforti-Ferrario, M. Banja, H. Bloem, R. L. Arantegui and M. Szabo, *PV Status Report 2012*, Institute for Energy, Renewable Energy Unit, European Commission, 2012.
7 A. Jäger-Waldau, *PV Status Report 2011*, Institute for Energy, Renewable Energy Unit, European Commission, 2011.
8 C. J. Brabec, *Sol. Energy Mater. Sol. Cells*, 2004, **83**, 273.
9 C. J. Brabec, N. S. Sariciftci and J. C. Hummelen, *Adv. Funct. Mater.*, 2001, **11**, 15.
10 H. Hoppe and N. S. Sariciftci, *J. Mater. Res.*, 2004, **19**, 1924.
11 B. C. Thompson and J. M. J. Fréchet, *Angew. Chem., Int. Ed.*, 2008, **47**, 58.
12 C. J. Brabec, J. A. Hauch, P. Schilinsky and C. Waldauf, *MRS Bull.*, 2005, **30**, 50.
13 C. J. Brabec and J. R. Durrant, *MRS Bull.*, 2008, **33**, 670.
14 H.-Y. Chen, J. Hou, S. Zhang, Y. Liang, G. Yang, Y. Yang, L. Yu, Y. Wu and G. Li, *Nat. Photonics*, 2009, **3**, 649.
15 T.-Y. Chu, J. Lu, S. Beaupr, Y. Zhang, J.-R. Pouliot, S. Wakim, J. Zhou, M. Leclerc, Z. Li, J. Ding and Y. Tao, *J. Am. Chem. Soc.*, 2011, **133**, 4250.
16 H. Zhou, L. Yang, A. C. Stuart, S. C. Price, S. Liu and W. You, *Angew. Chem., Int. Ed.*, 2011, **50**, 2995.
17 T. Ameri, G. Dennler, C. Lungenschmied and C. J. Brabec, *Energy Environ. Sci.*, 2009, **2**, 347.
18 S. Shockley and H. J. Queisser, *J. Appl. Phys.*, 1961, **32**, 510.
19 J. Frenkel, *Phys. Rev.*, 1931, **37**, 17.
20 W. Y. Liang, *Phys. Educ.*, 1970, **5**, 226.
21 J. L. Brédas, D. Beljonne, V. Coropceanu and J. Cornil, *Chem. Rev.*, 2004, **104**, 4917.
22 A. Cravino, *Appl. Phys. Lett.*, 2007, **91**, 243502.
23 K. Vandewal, A. Gadisa, W. D. Oosterbaan, S. Bertho, F. Banishoeib, I. V. Severen, L. Lutsen, T. J. Cleij, D. Vanderzande and J. V. Manca, *Adv. Funct. Mater.*, 2008, **18**, 2064.
24 M. Gruber, J. Wagner, K. Klein, U. Hörmann, A. Opitz, M. Stutzmann and W. Brütting, *Adv. Energy Mater.*, 2012, **2**, 1100.
25 M. C. Scharber, D. Mühlbacher, M. Koppe, P. Denk, C. Waldauf, J. Heeger and C. J. Brabec, *Adv. Mater.*, 2006, **18**, 789.
26 M. A. Green, K. Emery, Y. Hishikawa, W. Warta and E. D. Dunlop, *Prog. Photovoltaics*, 2012, **20**, 12; M. A. Green, K. Emery, Y. Hishikawa, W. Warta and E. D. Dunlop, *Prog. Photovoltaics*, 2013, **21**, 1.
27 A. De Vos, *J. Phys. D: Appl. Phys.*, 1980, **13**, 839.
28 G. Dennler, M. C. Scharber, T. Ameri, P. Denk, K. Forberich, C. Waldauf and C. J. Brabec, *Adv. Mater.*, 2008, **20**, 579.
29 K. M. Coakley and M. D. McGehee, *Chem. Mater.*, 2004, **16**, 4533.
30 A. Moliton and J. M. Nunzi, *Polym. Int.*, 2006, **55**, 583.
31 L. J. A. Koster, V. D. Mihailetchi and P. W. M. Blom, *Appl. Phys. Lett.*, 2006, **88**, 3.
32 B. P. Rand, D. P. Burk and S. R. Forrest, *Phys. Rev. B: Condens. Matter Mater. Phys.*, 2007, 75.
33 R. R. Lunt, T. P. Osedach, P. R. Brown, J. A. Rowehl and V. Bulovic, *Adv. Mater.*, 2011, **23**, 5712.
34 B. Minnaert and P. Veelaert, *Materials*, 2012, **5**, 1933.
35 T. Ameri, G. Dennler, C. Waldauf, P. Denk, K. Forberich, M. C. Scharber, C. J. Brabec and K. Hingerl, *J. Appl. Phys.*, 2008, **103**, 084506.
36 M. K. Siddiki, J. Li, D. Galipeau and Q. Qiao, *Energy Environ. Sci.*, 2010, **3**, 867–883.
37 S. Sista, Z. Hong, L.-M. Chen and Y. Yang, *Energy Environ. Sci.*, 2011, **4**, 1606–1620.
38 S.-I. Na, S.-S. Kim, J. Jo and D.-Y. Kim, *Adv. Mater.*, 2008, **20**, 4061.
39 D. Alemu, H.-Y. Wei, K.-C. Ho and C. W. Chu, *Energy Environ. Sci.*, 2012, **5**, 9662.
40 C.-C. Chen, L. Dou, R. Zhu, C.-H. Chung, T.-B. Song, Y. B. Zheng, S. Hawks, G. Li, P. S. Weiss and Y. Yang, *ACS Nano*, 2012, **6**, 7185.

41 J. Krantz, T. Stubhan, M. Richter, S. Spallek, I. Litzov, G. J. Matt, E. Spiecker and C. J. Brabec, *Adv. Funct. Mater.*, 2012, **23**, 1711.
42 F. Guo, X. Zhu, K. Forberich, J. Krantz, M. Salinas, M. Halik, S. Spallek, B. Butz, E. Spiecker, T. Ameri, N. Li, P. Kubis, D. M. Guldi, G. J. Matt and C. J. Brabec, *Adv. Energy Mater.*, 2013, DOI: 10.1002/aenm.201300100.
43 G. Dennler, H.-J. Prall, R. Koeppe, M. Egginger, R. Autengruber and N. S. Sariciftci, *Appl. Phys. Lett.*, 2006, **89**, 73502.
44 A. Colsmann, J. Junge, C. Kayser and U. Lemmer, *Appl. Phys. Lett.*, 2006, **89**, 203506.
45 A. G. F. Janssen, T. Riedl, S. Hamwi, H.-H. Johannes and W. Kowalsky, *Appl. Phys. Lett.*, 2007, **91**, 073519.
46 A. Hadipour, B. de Boer, J. Wildeman, F. B. Kooistra, J. C. Hummelen, M. G. R. Turbiez, M. M. Wienk, R. A. J. Janssen and P. W. M. Blom, *Adv. Funct. Mater.*, 2006, **16**, 1897.
47 X. W. Sun, D. W. Zhao, L. Ke, A. K. K. Kyaw, G. Q. Lo and D. L. Kwong, *Appl. Phys. Lett.*, 2010, **97**, 053303.
48 Y. Yuan, J. Huang and G. Li, *Green*, 2011, **1**, 65.
49 J. Ajuria, I. Etxebarria, W. Cambarau, U. Munecas, R. Tena-Zaera, J. C. Jimenoc and R. Pacios, *Energy Environ. Sci.*, 2011, **4**, 453.
50 S. Olthof, R. Timmreck, M. Riede and K. Leo, *Appl. Phys. Lett.*, 2012, **100**, 113302.
51 N. Li, T. Stubhan, J. Krantz, F. Machui, T. Ameri and C. J. Brabec, *Adv. Mater.*, 2013, submitted.
52 J. Y. Kim, K. Lee, N. E. Coates, D. Moses, T.-Q. Nguyen, M. Dante and A. J. Heeger, *Science*, 2007, **317**, 222.
53 J. Yang, R. Zhu, Z. Hong, Y. He, A. Kumar, Y. Li and Y. Yang, *Adv. Mater.*, 2011, **23**, 3465.
54 L. Dou, J. You, J. Yang, C.-C. Chen, Y. He, S. Murase, T. Moriarty, K. Emery, G. Li and Y. Yang, *Nat. Photonics*, 2012, **6**, 180.
55 J. Gilot, M. M. Wienk and R. A. J. Janssen, *Appl. Phys. Lett.*, 2007, **90**, 143512.
56 V. S. Gevaerts, A. Furlan, M. M. Wienk, M. Turbiez and R. A. J. Janssen, *Adv. Mater.*, 2012, **24**, 2130.
57 S. Kouijzer, S. Esiner, C. H. Frijters, M. Turbiez, M. M. Wienk and R. A. J. Janssen, *Adv. Energy Mater.*, 2012, **2**, 945.
58 N. Li, T. Stubhan, D. Baran, J. Min, H. Wang, T. Ameri and C. J. Brabec, *Adv. Energy Mater.*, 2012, **3**, 301.
59 Y. Zhou, C. Fuentes-Hernandez, J. Shim, J. Meyer, A. J. Giordano, H. Li, P. Winget, T. Papadopoulos, H. Cheun, J. Kim, M. Fenoll, A. Dindar, W. Haske, E. Najafabadi, T. M. Khan, H. Sojoudi, S. Barlow, S. Graham, J.-L. Brédas, S. R. Marder, A. Kahn and B. Kippelen, *Science*, 2012, **336**, 327.
60 Y. Zhou, C. Fuentes-Hernandez, J. W. Shim, T. M. Khan and B. Kippelen, *Energy Environ. Sci.*, 2012, **5**, 9827.
61 J. Yang, J. You, C.-C. Chen, W.-C. Hsu, H.-r. Tan, X. W. Zhang, Z. Hong and Y. Yang, *ACS Nano*, 2011, **5**, 6210.
62 P. Lalanne and G. M. Morris, *J. Opt. Soc.Am. A*, 1996, **13**, 779.
63 J. P. Hugonin and P. Lalanne, *Reticolo software for grating analysis*, Institut d'Optique, Orsay, France, 2005.
64 N.-K. Persson and O. Inganas, *Sol. Energy Mater. Sol. Cells*, 2006, **90**, 3491.
65 Z. Knittl, *Optics of Thin Films*, Wiley, London, 1976.
66 L. A. A. Pettersson, L. S. Roman and O. Inganas, *J. Appl. Phys.*, 1999, **86**, 487.
67 H. Hoppe, N. Arnold, D. Meissner and N. S. Sariciftci, *Thin Solid Films*, 2004, **589**, 451.
68 G. Dennler, K. Forberich, T. Ameri, C. Waldauf, P. Denk, C. J. Brabec, K. Hingerl and A. J. Heeger, *J. Appl. Phys.*, 2007, **102**, 123109.
69 M. Hiramoto, M. Suezaki and M. Yokoyama, *Chem. Lett.*, 1990, 327.
70 D. J. D. Moet, P. de Bruyn and P. W. M. Blom, *Appl. Phys. Lett.*, 2010, **96**, 153504.
71 D. J. D. Moet, P. de Bruyn, J. D. Kotlarski and P. W. M. Blom, *Org. Electron.*, 2010, **11**, 1821.
72 J. Gilot, M. M. Wienk and R. A. J. Janssen, *Adv. Mater.*, 2010, **22**, E67.
73 A. Hadipour, B. de Boer and P. W. M. Blom, *Org. Electron.*, 2008, **9**, 617.
74 J. Sakai, K. Kawano, T. Yamanari, T. Taima, Y. Yoshida, A. Fujii and M. Ozaki, *Sol. Energy Mater. Sol. Cells*, 2010, **94**, 376.
75 G. Li, V. Shrotriya, J. Huangi, Y. Yao, T. Moriarty, K. Emery and Y. Yang, *Nat. Mater.*, 2005, **4**, 864.
76 V. D. Mihailetchi, H. Xie, B. Boer, L. M. Popescu, J. C. Hummelen, P. W. M. Blom and L. J. A. Koster, *Appl. Phys. Lett.*, 2006, **89**, 012107.
77 K. Kawano, J. Sakai, M. Yahiro and C. Adachi, *Sol. Energy Mater. Sol. Cells*, 2009, **93**, 514.
78 C. H. Chou, W. L. Kwan, Z. Hong, L. M. Chen and Y. Yang, *Adv. Mater.*, 2011, **23**, 1282.
79 S. Sista, M. H. Park, Z. Hong, Y. Wu, J. Hou, W. L. Kwan, G. Li and Y. Yang, *Adv. Mater.*, 2010, **22**, 380.
80 B. P. Rand, P. Peumans and S. R. Forrest, *J. Appl. Phys.*, 2004, **96**, 7519.
81 N. Blouin, A. Michaud and M. Leclerc, *Adv. Mater.*, 2007, **19**, 2295.
82 S. H. Park, A. Roy, S. Beaupre, S. Cho, N. Coates, J. S. Moon, D. Moses, M. Leclerc, K. Lee and A. J. Heeger, *Nat. Photonics*, 2009, **3**, 297.
83 S. Alem, T.-Y. Chu, S. C. Tse, S. Wakim, J. Lu, R. Movileanu, Y. Tao, F. Belanger, D. Desilets, S. Beaupre, M. Leclerc, S. Rodman, D. Waller and R. Gaudiana, *Org. Electron.*, 2011, **12**, 1788.
84 Y. Sun, C. J. Takacs, S. R. Cowan, J. H. Seo, X. Gong, A. Roy and A. J. Heeger, *Adv. Mater.*, 2011, **23**, 2226.
85 L. Bürgi, M. Turbiez, R. Pfeiffer, F. Bienewald, H. J. Kirner and C. Winnewisser, *Adv. Mater.*, 2008, **20**, 2217.
86 J. C. Bijleveld, A. P. Zoombelt, S. G. J. Mathijssen, M. M. Wienk, M. Turbiez, D. M. de Leeuw and R. A. J. Janssen, *J. Am. Chem. Soc.*, 2009, **131**, 16616.
87 M. Dueggeli, M. Zaher Eteish, P. Hayoz, O. F. Aebischer, M. Fonrodona Turon and M. G. R. Turbiez, *PCT Int. Appl.*, 2010, WO 2010049323.
88 Z. Yi, X. Sun, Y. Zhao, Y. Guo, X. Chen, J. Qin, G. Yu and Y. Liu, *Chem. Mater.*, 2012, **24**, 4350.

89 S. Kouijzer, S. Esiner, C. H. Frijters, M. Turbiez, M. M. Wienk and R. A. J. Janssen, *Adv. Energy Mater.*, 2012, **2**, 945.
90 Y. Zhou, J. W. Shim, C. Fuentes-Hernandez, A. Sharma, K. A. Knauer, A. J. Giordano, S. R. Marder and B. Kippelen, *Phys. Chem. Chem. Phys.*, 2012, **14**, 12014.
91 L. Dou, W.-H. Chang, J. Gao, C.-C. Chen, J. You and Y. Yang, *Adv. Mater.*, 2013, **25**, 825.
92 J. You, L. Dou, K. Yoshimura, T. Kato, K. Ohya, T. Moriarty, K. Emery, C.-C. Chen, J. Gao, G. Li and Y. Yang, *Nat. Commun.*, 2013, **4**, 1446.
93 M. Riede, C. Uhrich, J. Widmer, R. Timmreck, D. Wynands, G. Schwartz, W. M. Gnehr, D. Hildebrandt, A. Weiss, J. Hwang, S. Sudharka, P. Erk, M. Pfeiffer and K. Leo, *Adv. Funct. Mater.*, 2011, **21**, 3019.
94 B. E. Lassiter, J. D. Zimmerman, A. Panda, X. Xiao and S. R. Forrest, *Appl. Phys. Lett.*, 2012, **101**, 063303.
95 G. Wei, X. Xiao, S. Wang, K. Sun, K. J. Bergemann, M. E. Thompson and S. R. Forrest, *ACS Nano*, 2011, **6**, 972.
96 R. Pandey and R. J. Holmes, *Adv. Mater.*, 2010, **22**, 5301.
97 130116_PR_Heliatek_achieves_record_cell_effiency_for_OPV.pdf.
98 J. H. Seo, D.-H. Kim, S.-H. Kwon, M. Song, M.-S. Choi, S. Y. Ryu, H. W. Lee, Y. C. Park, J.-D. Kwon, K.-S. Nam, Y. Jeong, J.-W. Kang and C. S. Kim, *Adv. Mater.*, 2012, **24**, 4523.
99 S. Sista, Z. Hong, M.-H. Park, Z. Xu and Y. Yang, *Adv. Mater.*, 2010, **22**, E77.
100 Z. Tang, Z. George, Z. Ma, J. Bergqvist, K. Tvingstedt, K. Vandewal, E. Wang, L. M. Andersson, M. R. Andersson, F. Zhang and O. Inganäs, *Adv. Energy Mater.*, 2012, **2**, 1467.
101 M. A. Green, *Solid-State Electron.*, 1981, **24**, 788.
102 M. A. Green, *Sol. Cells*, 1982, **7**, 337.
103 S. W. Tong, Y. Wang, Y. Zheng, M.-F. Ng and K. P. Loh, *Adv. Funct. Mater.*, 2011, **21**, 4430.
104 V. C. Tung, J. Kim, L. J. Cote and J. Huang, *J. Am. Chem. Soc.*, 2011, **133**, 9262.
105 W. S. Hummers and R. E. Offeman, *J. Am. Chem. Soc.*, 1958, **80**, 1339.
106 J. Kim, V. C. Tung and J. Huang, *Adv. Energy Mater.*, 2011, **1**, 1052.
107 V. C. Tung, J. Kim and J. Huang, *Adv. Energy Mater.*, 2012, **2**, 299.
108 K. Bücher and A. Schönecker, *Eur. Photovoltaic Sol. Energy Conf.*, 1991, 107.
109 J. Burdick and T. Glatfelter, *Sol. Cells*, 1986, **18**, 301.
110 M. Meusel, C. Baur, G. Letay, A. W. Bett, W. Warta and E. Fernandez, *Prog. Photovoltaics*, 2003, **11**, 499.
111 R. L. Mueller, *Sol. Energy Mater. Sol. Cells*, 1993, **30**, 37.
112 Y. Nakata and T. Inoguchi, *Optoelectron.–Devices Technol*, 1989, **4**, 75.
113 D. Ran, S. Zhang, J. Zhang, X. Zhang and F. Wan, *SPIE-Int. Soc. Opt. Eng., Proc.*, 2007, **6723**, 672316.
114 G. Dennler, H.-J. Prall, R. Koeppe, M. Egginger, R. Autengruber and N. S. Sariciftci, *Appl. Phys. Lett.*, 2006, **89**, 073502.
115 P. Peumans, S. Uchida and S. R. Forrest, *Nature*, 2003, **425**, 158.
116 J. Gilot, M. M. Wienk and R. A. J. Janssen, *Adv. Funct. Mater.*, 2010, **20**, 3904.
117 J. M. Kroon, M. M. Wienk, W. J. H. Verhees and J. C. Hummelen, *Thin Solid Films*, 2002, **223**, 403.
118 J. Gilot, M. M. Wienk and R. A. J. Janssen, *Org. Electron.*, 2011, **12**, 660.
119 Z. E. Ooi, R. Jin, J. Huang, Y. F. Yoo, A. Sellinger and J. C. De Mello, *J. Mater. Chem.*, 2008, **18**, 1644.